

MESOSCALE MODELING OF BIOMIMETIC MACROMOLECULAR  
AGGREGATES

by

GEETARTHA UPPALADADIUM

A thesis submitted to the

Graduate School – New Brunswick

Rutgers, The State University of New Jersey

In partial fulfillment of the requirements

For the degree of

Master of Science

Graduate Program in Chemical and Biochemical Engineering

Written under the direction of

Dr. Meenakshi Dutt

And approved by

---

---

---

New Brunswick, New Jersey

May, 2016

## **ABSTRACT OF THE THESIS**

MESOSCALE MODELING OF BIOMIMETIC MACROMOLECULAR

AGGREGATES

By GEETARTHA UPPALADADIUM

Thesis Director:

Dr. Meenakshi Dutt

Drug carriers are designed with an aim of decent pharmacokinetics and interaction with various nanoparticles. Several characteristics of drug carriers like shape and size influence the pharmacokinetics and interaction. To understand the factors that affect the morphology and dynamics of the system, we design coarse-grained models for the constituents of the carriers. Capturing the physical phenomena would require a molecular simulation technique capable of resolving over a vast ranges of space and time. Dissipative Particle dynamics (DPD) is one such technique which can simultaneously resolve molecular and continuum scales. This technique can handle large length (from 1 nm up to 1  $\mu\text{m}$ ) and time scales (nano-seconds to micro-seconds). This thesis focuses on understanding the underlying mechanisms that affect the organization, shape, stiffness and interfacial stability of biomaterials. This will help design simple biomimetic

macromolecules finding use in delivery of therapeutic agents and cellular sensing. It also helps in understanding the underlying mechanisms of interactions between micelles, proteins or synthetic particles with bio-inspired macromolecules.

## **Acknowledgements**

I would like to extend my deepest appreciation and gratitude to Dr. Meenakshi Dutt for being an excellent mentor during my work in Computational Hybrid Soft materials Laboratory. Her involvement in every step of the project encouraged me to be more productive in the time I worked with the group. She also encouraged me to participate in projects in collaboration with other research groups. This exposed me to diverse work cultures in the field of scientific research. She always encouraged me to present our work in group meetings, various conferences and poster sessions. Additionally, I also had an opportunity to assist her in teaching Chemical Engineering Thermodynamics to undergraduate students. She gave me an opportunity to present my work to her students, so that the students understand the underlying principles of thermodynamics in my research as well as the students get an idea of how scientific research is carried out. Such a dedication and commitment will always be an inspiration for me.

I would also like to thank Dr. Fikret Aydin for being a great colleague. Fikret has worked with me on all projects that I worked on in Dr. Dutt's group. He was always available for help whenever I needed it. I can recollect instances when I called him up past midnight and he answered my calls. Along with being a great colleague, he is also a very dear friend. I would also like to thank Xiaolei Chu from Dr. Dutt's group for working with me on multiple projects beyond the scope of this thesis.

I am thankful to Dr. Charles Roth and Dr. Shishir Chundawat for accepting to be on the Thesis Committee.

## Table of Contents

<b>TITLE PAGE</b>	<b>i</b>
<b>ABSTRACT OF THE THESIS</b>	<b>ii</b>
<b>Acknowledgements</b>	<b>iv</b>
<b>Table of Contents</b>	<b>v</b>
<b>List of Tables</b>	<b>vii</b>
<b>List of Figures</b>	<b>ix</b>
<b>Chapter 1 Introduction</b>	<b>1</b>
<b>Chapter 2 Methodology</b>	<b>4</b>
<b>Chapter 3 Designing Hairy Vesicles: Role of Molecular Architecture, Composition and Volumetric Confinement</b>	<b>7</b>
<b>3.1 Overview</b>	<b>7</b>
<b>3.2 Model and system setup</b>	<b>8</b>
3.2.1 Role of Molecular Architecture in Bulk Conditions	8
3.2.2 Role of Confinement	10
<b>3.3 Results and Discussions</b>	<b>12</b>
3.3.1 Aggregation dynamics influenced by intrinsic factors	12
3.3.2 Aggregation dynamics influenced by extrinsic factors	16
3.3.3 Tether distribution	18
3.3.4 Morphology influenced by intrinsic factors	21
3.3.5 Morphology influenced by extrinsic factors	30

<b>3.4 Chapter Conclusions</b>	<b>35</b>
<b>Chapter 4 Interactions of Bald and Hairy Vesicles with Nanoparticles</b>	<b>37</b>
<b>4.1 General Overview</b>	<b>37</b>
<b>4.2 Adsorption of functionalized NPs onto bald vesicle surface</b>	<b>38</b>
4.2.1 Modeling and system setup	38
4.2.2 Results and Discussions	40
<b>4.3 Effect of grafted tethers on Adsorption</b>	<b>46</b>
4.3.1 System description	46
4.3.2 NP patch- Phospholipid head group interaction driven adsorption	47
4.3.3 NP patch- Tether interaction driven adsorption	57
<b>4.4 Chapter Conclusions</b>	<b>61</b>
<b>Chapter 5 Conclusions</b>	<b>62</b>
<b>References</b>	<b>64</b>

## List of Tables

Table 3.1: Table of the scaling exponents $\alpha$ and $\beta$ for the self-assembly of binary mixtures composed of different relative concentrations of hairy lipid and phospholipid molecules, and length of the tethers .....	14
Table 3.2: The number of hairy lipid molecules and the radius of gyration of the tethers present in the inner and outer monolayers of the self-assembled vesicles, and maximum and minimum distances from the center of mass of the vesicle to the lipid head groups in the outer monolayer for different relative concentrations of the hairy lipids and tether lengths.....	19
Table 3.3: The radius of gyration of the tethers presents in the inner and outer monolayers of the self-assembled vesicles for different relative concentrations of the hairy lipids and tether lengths in the confinement with a channel height of $10r_c$ , $15r_c$ and $20r_c$ .....	20
Table 3.4: The number of hairy lipid molecules present in the inner and outer monolayers of the self-assembled vesicles for different relative concentrations of the hairy lipids and tether lengths at different degrees of confinement.....	21
Table 3.5: Table of the scaling exponents $\alpha$ and $\beta$ for the coarsening dynamics in the bilayer of a binary hairy vesicle induced by the dissimilarity of the hydrocarbon tail groups of the phospholipid and hairy lipids, for different tether lengths.....	27
Table 3.6: The area per hairy lipid for tethers composed of three and six beads in the inner and outer monolayers of the binary hairy vesicle as a function of the inter-specie tail-tail soft repulsive interaction parameters $a_{i12}$ .....	28

Table 3.7: The reduced volume and the x, y, z - principal axes of the self-assembled hairy vesicles for different relative concentrations of the hairy lipids and tether lengths in bulk conditions (without walls).....	31
Table 3.8: The total outer surface area and enclosed volume of the self-assembled hairy vesicles for different relative concentrations of the hairy lipids and tether lengths at different degrees of confinement.....	32
Table 3.9: The x, y, z - principal axes of the self-assembled hairy vesicles for different relative concentrations of the hairy lipids and tether lengths in the confinement with a channel height of $8r_c$ , $10r_c$ , $15r_c$ and $20r_c$ .....	34
Table 4.1: Soft repulsive interaction parameters, $a_{ij}$ between moieties of the system where ‘i’ represents the species in the columns and ‘j’ represents the species in the rows.....	39
Table 4.2: A comparison of the dimensions of the liposomes for different patch sizes of NPs at end of simulation.....	44

## List of Figures

Figure 3.1: Images of the (a) amphiphilic phospholipid molecule, (b) hairy lipid molecule with a tether composed of three beads, and (c) hairy lipid molecule with a tether composed of six beads. (d) Time evolution of the average total energy of binary component hairy vesicle composed of phospholipids (90%) and hairy lipid molecules with tether composed of three beads (10%), and the corresponding images of the aggregation process. (e) An image of a stable self-assembled binary hairy vesicle composed of phospholipids (90%) and hairy lipid molecules with tethers composed of three beads (10%) at time  $t = 60,000\tau$ .....**9**

Figure 3.2: (a) The dimensions of the three-dimensional simulation box and channel used to confine the amphiphilic molecules. (b) The initial system configuration for a mixture of phospholipid and hairy lipid molecules in the confinement with a channel height of  $15r_c$ . (c) A side, (d) top and (e) cross-sectional view of a self-assembled prolate vesicle in the confinement with a channel height of  $20r_c$  at time  $t = 120,000\tau$ . (f) A side, (g) top and (h) cross-sectional view of a self-assembled oblate vesicle in the confinement with a channel height of  $10r_c$  at time  $t = 120,000\tau$ . (i) A side, (j) top and (k) cross-sectional view of a self-assembled bicelle in the confinement with a channel height of  $8r_c$  at time  $t = 120,000\tau$ . The systems in (b) – (k) are composed of phospholipids (90%) and hairy lipid molecules with tethers composed of three beads (10%). The wall beads are reduced in size to enhance the top view of the different vesicle morphologies.....**11**

Figure 3.3: The time evolution (beginning from time  $t = 1,000\tau$ ) of the total number of clusters encompassing mixtures of phospholipids and hairy lipids with tethers composed of (a) three beads, for relative concentration of the hairy lipids given by 10%, 20%, 30%,

40% and 50%, and (b) six beads, for relative concentration of the hairy lipids given by 10% and 20%. The inset in (a) and (b) show the time evolution of the total number of clusters between the time interval  $t = 0$  and  $t = 1,000\tau$ . (c) The time evolution for the average cluster size for mixtures of phospholipids and hairy lipid molecules with the tethers composed of (c) three beads, for relative concentration of the hairy lipids given by 10%, 20%, 30%, 40% and 50%, and (d) six beads, for relative concentration of the hairy lipid given by 10% and 20%.....**15**

Figure 3.4: A plot of the scaling exponent  $\alpha$  as a function of the distance between two planar surfaces for the self-assembly of binary mixtures composed of different relative concentrations of hairy lipid and phospholipid molecules, and length of the tethers.....**18**

Figure 3.5: Equilibrium configurations of the binary hairy vesicle composed of a range of concentrations of the hairy lipids (10% to 50% for the short tethers and 10% to 20% for the long tethers) at  $t = 5,000\tau$ , for different hydrocarbon chain stiffness of the phospholipid specie given by  $K_{\text{angle}} = 5, 10, 15, \text{ and } 20$ . The angle coefficient of the hairy lipid hydrocarbon chain was set at  $K_{\text{angle}} = 0$ .....**23**

Figure 3.6: The phase diagram for the reduced volume of the self-assembled hairy vesicles with tethers composed of (a) three beads, (b) six beads as a function of  $x_{\text{tether}}$  and  $K_{\text{angle}}$ . The phase diagram for the  $r_{\text{min}}/r_{\text{max}}$  of the self-assembled hairy vesicles with tethers composed of (c) three beads, (d) six beads as a function of  $x_{\text{tether}}$  and  $K_{\text{angle}}$ . The phase diagram for the interfacial line tension of the self-assembled hairy vesicles with tethers composed of (e) three beads, (f) six beads as a function of  $x_{\text{tether}}$  and  $K_{\text{angle}}$ .  $x_{\text{tether}}$  is varied from 0.1 to 0.5 for lipid species with short tethers and from 0.1 to 0.2 for lipid species with long tethers.  $K_{\text{angle}}$  for the phospholipids is varied from 5 to 20.....**24**

Figure 3.7: A plot of the time evolution of the total number of clusters of the hairy lipid molecules with (a) short and (b) long tethers. A plot of the time evolution for the average size of the clusters composed of hairy lipids with (c) short and (d) long tethers. All the simulations start from a completely mixed state. The inter-specie tail-tail soft repulsive interaction parameter was set at the following values:  $a_{t1t2} = 31, 32, 35, 38, 41,$  and  $50$ . **26**

Figure 3.8: Final configurations of the binary hairy vesicle at time  $t = 10,000\tau$  for different soft repulsive interaction parameters between the tail groups of the phospholipids and hairy lipids given by (a)  $a_{t1t2} = 31,$  (b)  $a_{t1t2} = 50,$  and (c)  $a_{t1t2} = 31,$  (d)  $a_{t1t2} = 50,$  respectively for short and long tethers. Plots of the (e) minimum and maximum distance of the lipid head beads from the COM of vesicle, and (f) average line tension as function of  $a_{t1t2}$ . **29**

Figure 3.9: A plot of the reduced volume of the self-assembled hairy vesicles as a function of the distance between two planar surfaces for different relative concentrations of the hairy lipids and tether lengths. **31**

Figure 3.10: An image that shows the principal axes (x, y and z) of the self-assembled binary hairy vesicle with a prolate morphology. **33**

Figure 3.11: A plot of interfacial line tension of the self-assembled hairy vesicles as a function of tether concentration for different distances between two planar surfaces and different tether lengths. **35**

Figure 4.1: Coarse-grained structure of individual species present in the bald vesicle-NP system. **39**

Figure 4.2: Initial configuration of the bald vesicle-NP system. **41**

Figure 4.3: Increase of number of contacts with time until $40000 \tau$ between liposome and NPs with patch size <b>a)</b> 10%, <b>b)</b> 30%, <b>c)</b> 50%.....	<b>42</b>
Figure 4.4: Residence time measurements of NPs with patch sizes of (a) 10%, (b) 30%, (c) 50% following their adsorption on to the phospholipid head groups.....	<b>44</b>
Figure 4.5: Binding of nanoparticles to the liposome surface causes reorientation of the lipid head groups reducing the area per lipid of the molecule.....	<b>45</b>
Figure 4.6: Spherical patchy NP with a radius of $2.25r_c$ .....	<b>46</b>
Figure 4.7: Initial configuration of (a) binary component hairy vesicle composed of phospholipids (50%) and hairy lipid molecules with short tethers (50%), and 4 NPs placed outside the interaction range of the hairy vesicle, (b) binary component hairy vesicle composed of phospholipids (50%) and hairy lipid molecules with long tethers (50%), and 4 NPs placed outside the interaction range of the hairy vesicle, (c) short tether hairy vesicle with 4 NPs adsorbed onto the phospholipid head groups at $t = 160,000\tau$ , (d) long tether hairy vesicle with 4 NPs adsorbed onto the phospholipid head groups at $t = 160,000\tau$ .....	<b>48</b>
Figure 4.8: A plot of number of interactions between nanoparticle and tethers as a function of time for 4 nanoparticles interacting with hairy vesicle composed of long tethers.....	<b>49</b>
Figure 4.9: Images of the capture of a single NP by phospholipid head groups of a hairy vesicle composed of long tethers at (a) $t = 2130\tau$ , (b) $t = 2230\tau$ , (c) $t = 2300\tau$ , (d) $t = 2320\tau$ , (e) $t = 2340\tau$ , (f) $t = 2380\tau$ and (g) a plot of the number of interactions between NP patch and tethers as a function of time during the capturing process.....	<b>51</b>

Figure 4.10: Plots of the number of interactions between the NP patch and phospholipid head groups as a function of time for 4 NPs interacting with hairy vesicle composed of (a) short and (b) long tethers. The simulations of hairy vesicles composed of short and long tethers have been run for a total time of  $80,000\tau$  and  $160,000\tau$ , respectively. The measurements from four simulation runs using different random seeds are shown separately in the plot.....**52**

Figure 4.11: Plots of number of interactions between nanoparticle patch and phospholipid head groups as a function of time for (a) 8, (b) 12 nanoparticles interacting with hairy vesicle composed of short tethers and (c) 8, (d) 12 nanoparticles interacting with hairy vesicle composed of long tethers. The simulations of hairy vesicles composed of short and long tethers have been run for a total time of  $80,000\tau$  and  $160,000\tau$ , respectively. The measurements of four simulation runs using different random seeds are shown separately in the plot.....**53**

Figure 4.12: A plot of the number of NPs adsorbed on to the phospholipid head groups of hairy vesicle composed of short and long tethers as a function of tether composition (0.1 to 0.5) respectively for the NP radius of  $0.75r_c$  and  $1.50r_c$ , and the NP radius of  $1.50r_c$  and  $2.25r_c$ . The simulations have been run for a total time of  $30,000\tau$  and each data point has been averaged over four simulation runs using different random seeds.....**54**

Figure 4.13: Residence time measurements of NPs after their adsorption on to the phospholipid head groups of hairy vesicle composed of short and long tethers for (a) 4, (b) 8 and (c) 12 NPs.....**56**

Figure 4.14: Images of the capture of single NP by tethers of hairy vesicle composed of long tethers at (a)  $t = 95\tau$ , (b)  $t = 125\tau$ , (c)  $t = 130\tau$ , (d)  $t = 180\tau$ , and (e) a plot of number of interactions between NP patch and tethers as a function of time during the capturing process.....**58**

Figure 4.15: Plots of number of interactions between NP patch and tethers as a function of time for (a) 4, (b) 8, (c) 12 NPs interacting with hairy vesicle composed of long tethers. The simulations have been run for a total time of  $80,000\tau$ . The measurements from four simulation runs using different random seeds are shown separately in the plot.....**59**

Figure 4.16: Residence time measurements of NPs following their adsorption on to the phospholipid head groups of the hairy vesicle composed of short tethers and tethers of hairy vesicles composed of long tethers for (a) 4, (b) 8 and (c) 12 NPs. The simulations have been run for a total time of  $10,000\tau$  and each data point has been averaged over four simulation runs using different random seeds.....**60**

## Chapter 1 Introduction

The plasma membranes of eukaryotic cells protect the protein and the lipid molecules in the non-cyclic monolayer from the external environment by a protective layer of carbohydrate molecules. These membranes are made of many amphiphilic molecules, of which phospholipid is a major component<sup>1</sup>. The phospholipids comprise of a hydrophilic head group and hydrophobic tail group. These molecules self-organize into aggregates and domains<sup>2-15</sup> owing to the conflicting chemistries of the head and tail groups. The ability of the cell membranes to reorganize its constituents facilitates many cellular functionalities like interfacial binding<sup>1,16</sup>, fusion, budding and aggregation<sup>17,18</sup>. Additionally, these molecules are known to promote processes like cell recognition, communication and adhesion which include sperm-egg interactions, blood clotting, lymphocyte recirculation and inflammatory responses.

One of the aims of this thesis is designing interfacial stable delivery vehicles with shapes that are favorable for an unhindered passage through the circulation system and efficient internalization by desired cell populations and understand the factors that affect the organization, shape, stiffness and interfacial stability. Shape of the carrier is a major parameter that needs attention to while designing them. The morphology of the vesicles is affected by various intrinsic and extrinsic factors. One of the intrinsic factors we discuss about is the stiffness of hydrocarbon tails. The stiffness of the hydrocarbon tails of lipid molecules is dependent upon their length and saturation.<sup>19-21</sup> The stiffness of the

amphiphilic constituents of the vesicle are known to affect the stability and bending rigidity of the lipid bilayers.<sup>20,22</sup> The circulation time and encapsulation efficiency of the carriers depends on the elasticity of the membranes.<sup>19,23</sup> Thus, chain stiffness is an important factor to be taken into consideration during the design of therapeutic agent carriers.

The carbohydrate chains on the surface of cells inspire the design of biocompatible therapeutic agent carriers of longer circulation times and targeted delivery.<sup>24-28</sup> A common practice to mimic this nature of cell surface is to graft Polyethylene glycol (PEG) chains to the lipid head groups.<sup>29-31</sup> Presence of PEG chains influences the size<sup>31-33</sup>, shape<sup>33-35</sup>, drug loading capability<sup>31,36,37</sup> of the liposomes. The shape of the equilibrated aggregates also depends on the spatial distribution of curvature-inducing functional groups present in the bilayer<sup>38-40</sup>.

In addition to intrinsic factors, extrinsic properties like volumetric confinement can also be used to control the shape of aggregates.<sup>22,41</sup> It has been found that dimensions, geometry, surface characteristics of the confining medium influence the morphology of equilibrated block copolymer aggregates.<sup>42-47</sup>

Simulations pertaining to lipid bilayers resolving the dynamics of the lipid and water molecules on an atomistic scale are computationally expensive. Hence, it is important to employ a suitable tool for addressing the phenomena occurring on a mesoscale. Methods like coarse-graining<sup>22,41,47,49-67</sup>, implicit solvent methods<sup>50-52,68-74</sup> or mean field theoretical approaches<sup>75-83</sup> can be used to resolve dynamics over large length and time scales. Previously implicit solvent approaches have been used to investigate phase segregation dynamics using Monte Carlo<sup>84</sup> and coarse-grained Molecular dynamics

(MD) technique.<sup>14</sup> However, we used a MD based approach entitled Dissipative Particle Dynamics (DPD)<sup>2,6,22,41,48,53-57,85-87</sup> which is capable of resolving both molecular and continuum scales simultaneously and capture hydrodynamic behavior, to study phase segregation in multi-component lipid vesicles.<sup>2,6,86,88-90</sup>

## Chapter 2 Methodology

Dissipative Particle Dynamics (DPD) is a mesoscopic simulation technique that uses soft-sphere coarse-grained models to capture both the molecular details of the nanoscopic building blocks and their supramolecular organization while simultaneously resolving the hydrodynamics of the system over extended time scales.<sup>41,91,92</sup> In order to capture the dynamics of the soft spheres, the DPD technique integrates Newton's equation of motion via the use of similar numerical integrators used in other deterministic particle-based simulation methods.<sup>91,93</sup> The force acting on a soft sphere  $i$  due to its interactions with a neighboring soft sphere  $j$  ( $j \neq i$ ) has three components: a conservative force, a dissipative force and a random force, which operate within a certain cut-off distance  $r_c$  from the reference particle  $i$ . These forces are pairwise additive and yield the total force acting on particle  $i$ , which is given by  $\mathbf{F}_i = \sum_{j \neq i} \mathbf{F}_{c,ij} + \mathbf{F}_{d,ij} + \mathbf{F}_{r,ij}$ . The soft spheres interact via a soft-repulsive force ( $\mathbf{F}_{c,ij} = a_{ij} (1 - \frac{r_{ij}}{r_c}) \hat{\mathbf{r}}_{ij}$ , for  $r_{ij} < r_c$  and  $\mathbf{F}_{c,ij} = 0$ , for  $r_{ij} \geq r_c$ ), a dissipative force ( $\mathbf{F}_{d,ij} = -\gamma \omega^d(r_{ij}) (\hat{\mathbf{r}}_{ij} \cdot \mathbf{v}_{ij}) \hat{\mathbf{r}}_{ij}$ ) and a random force ( $\mathbf{F}_{r,ij} = -\sigma \omega^r(r_{ij}) \theta_{ij} \hat{\mathbf{r}}_{ij}$ ), where  $\omega^d(r) = [w^r(r)]^2 = (1-r)^2$  (for  $r < 1$ ),  $\omega^d(r) = [w^r(r)]^2 = 0$  (for  $r \geq 1$ ) and  $\sigma^2 = 2\gamma k_B T$ .  $a_{ij}$  is the maximum repulsion between spheres  $i$  and  $j$ ,  $\mathbf{v}_{ij} = \mathbf{v}_i - \mathbf{v}_j$  is the relative velocity of the two spheres,  $r_{ij} = r_i - r_j$ ,  $r_{ij} = |r_i - r_j|$ ,  $\hat{\mathbf{r}}_{ij} = r_{ij}/r_{ij}$ ,  $r = r_{ij}/r_c$ ,  $\gamma$  is the viscosity related parameter used in the simulations,  $s$  is the noise amplitude,  $\theta_{ij}(t)$  is a randomly fluctuating variable from Gaussian statistics,  $\omega^d$  and  $\omega^r$  are the separation dependent weight functions which become zero at distances greater than or equal to the

cutoff distance  $r_c$ . Since the local linear and angular momentum is conserved by all of these three forces, even the small systems exhibit hydrodynamic behavior.<sup>91</sup> The constraints imposed on the random and dissipative forces by certain relations ensure that the statistical mechanics of the system conforms to the canonical ensemble.<sup>91,93</sup> The relation between the pair repulsion parameter  $a_{ij}$  and the Flory interaction parameter  $\chi$  for a bead number density  $\rho = 3r_c^{-3}$  is given by  $\chi = (0.286 \pm 0.002)(a_{ij} - a_{ii})$ .<sup>91</sup> Groot et al.<sup>91</sup> have provided a detailed explanation of the relationship between the Flory's  $\chi$  parameter and the DPD interaction parameters.

The soft repulsive pair potential parameters for the lipid molecule head and tail beads were selected to capture its amphiphilic nature.<sup>94</sup> In addition, the tether beads are considered to be hydrophilic in nature. The interaction parameters between the like components,  $a_{ij}$ , are based on the property of water.<sup>91</sup> The repulsion parameter between two beads of the same type is set at  $a_{ii} = 25$  (measured in units of  $k_B T / r_c$ ) which is based upon the compressibility of water at room temperature<sup>91</sup> for a bead density of  $\rho = 3r_c^{-3}$ . The soft repulsive interaction parameter  $a_{ij}$  between hydrophobic and hydrophilic beads is set at  $a_{ij} = 100 k_B T / r_c$ , and is determined by using the Flory-Huggins interaction parameters,  $\chi$ , as  $a_{ij} = a_{ii} + 3.496\chi$ , for  $\rho = 3r_c^{-3}$ .<sup>91</sup>

Two consecutive beads of a molecule are connected via a bond that is described by the harmonic spring potential  $E_{bond} = K_{bond}((r - b)/r_c)^2$ , where  $K_{bond}$  is the bond constant and  $b$  is the equilibrium bond length. The constants,  $K_{bond}$  and  $b$  are assigned values of  $64\epsilon$  and  $0.5r_c$ , respectively.<sup>41,57</sup> The three-body stiffness potential

along the lipid tails has the form  $E_{angle} = K_{angle}(1 + \cos\theta)$  where  $\theta$  is the angle formed by three adjacent beads. The coefficient  $K_{angle}$  is set to be  $20\epsilon$  in our simulations. The three-body stiffness term increases the stability and bending rigidity of the bilayers. Similar bond and angle potential functional forms and parameters are used for the tethers.

In our simulations, the respective characteristic length and energy scale are  $r_c$  and  $k_B T$ . As a result, our characteristic time scale can be described as  $\tau = \sqrt{mr_c^2 / k_B T}$ . Finally,  $\sigma = 3$  and  $\Delta t = 0.02\tau$  are used in the simulations along with the total bead number density of  $\rho = 3r_c^{-3}$  and a dimensionless value of  $r_c = 1$ .<sup>57</sup> The mass of all the beads is set to unity.<sup>41,57,59,88,91,92</sup>

We draw a correspondence between our model and physical systems via the experimental properties of biological lipid bilayers.<sup>92</sup> The characteristic length scale is  $r_c = 0.76$  nm, and is obtained through the comparison of experimental measurements of the interfacial area per lipid of a dipalmitoylphosphatidylcholine (DPPC) bilayer with similar measurements from our simulations. The time scale  $\tau$  was calculated to be 6.0 ns by comparing the experimental measurement of the diffusion coefficient of DPPC bilayer, which is given by  $5 \times 10^{-12}$  m<sup>2</sup>/s,<sup>57</sup> with that obtained from the simulations. Using a temperature of 50 °C, the energy scale is calculated to be  $\epsilon = k_B T = 4.5 \times 10^{-21}$  J.

## Chapter 3 Designing Hairy Vesicles: Role of Molecular Architecture, Composition and Volumetric Confinement

The publications relevant to details of the discussions provided in this section:

- Aydin, F., **Uppaladadium, G.**, Dutt, M., 2015, the design of shape-tunable hairy vesicles. *Colloids and Surfaces B: Biointerfaces* 128, 268-275.
- Aydin, F., **Uppaladadium, G.**, Dutt, M., 2015, Harnessing nanoscale confinement to design sterically stable vesicles of specific shapes via self-assembly. *J. Phys. Chem. B* 119 (32), 10207-10215.
- **Uppaladadium, G.**, Aydin, F., Chong, L. and Dutt M., *Review article in preparation.*

### Contribution to work:

- Running relevant simulations.
- Performing analysis and visualizing the system.

### 3.1 Overview

In this chapter, our primary focus will be on designing of interfacially stable hairy vesicles which act as drug carriers to target cell populations<sup>95</sup> and have a morphology promoting the circulation and internalization by target cells. The stability and morphology of these carriers greatly influences the drug delivery efficacy. The morphology of the aggregates is controlled by various intrinsic and extrinsic factors. Experimental and computational studies have investigated the morphology of binary mixtures of PEGylated and non-PEGylated lipids,<sup>33,37,95,96</sup> and their dynamics and

stability,<sup>29,95,96</sup> for species composed of the same hydrocarbon tail groups.<sup>31,33,36</sup> An effort has been made in this chapter to understand the effect of intrinsic factors like tether length, relative concentration of hairy lipids, molecular stiffness and extrinsic factors like volumetric confinement on cluster growth dynamics and aggregate morphology. For this purpose, a Molecular dynamics based mesoscopic simulation technique called Dissipative Particle Dynamics has been adopted to carry out investigations.

## **3.2 Model and system setup**

### **3.2.1 Role of Molecular Architecture in Bulk Conditions**

The constituents of the system are phospholipids, hairy lipids and solvent as shown in the Figure 3.1 (a). Bead-spring models represent these molecules. A phospholipid molecule is composed of three hydrophilic head groups and two hydrophobic tail groups containing three beads each. The hairy lipid molecules are essentially a phospholipid molecules with hydrophilic tethers grafted to one of the head beads. The hairs are modeled by three and six beads and are classified as short and long respectively. Experimental examples for the tethers are PEG chains with degrees of polymerization ( $n$ ) of 6 and 12 respectively. Previous theoretical<sup>97</sup> and experimental studies<sup>98,99</sup> demonstrate that polymers with 6 to 17 EO units to reduce amount of protein adsorption at a certain surface coverage because of the entropic repulsion offered by the tethers .

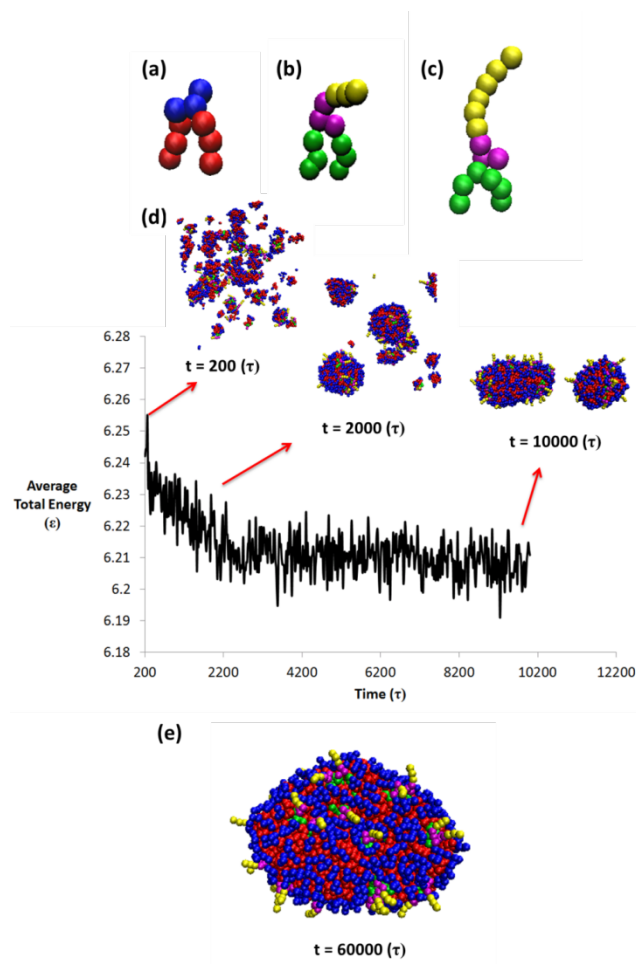


Figure 3.1: Images of the (a) amphiphilic phospholipid molecule, (b) hairy lipid molecule with a tether composed of three beads, and (c) hairy lipid molecule with a tether composed of six beads. (d) Time evolution of the average total energy of binary component hairy vesicle composed of phospholipids (90%) and hairy lipid molecules with tether composed of three beads (10%), and the corresponding images of the aggregation process. (e) An image of a stable self-assembled binary hairy vesicle composed of phospholipids (90%) and hairy lipid molecules with tethers composed of three beads (10%) at time  $t = 60,000\tau$

The soft repulsive pair potential parameters between different species are assigned the following values in order to capture the amphiphilic nature of species. The units for the parameters are  $k_B T / r_c$ .

$$a_{ss} = 25, a_{TT} = 25, a_{Ts} = 25, a_{h1h1} = 25, a_{t1t1} = 25, a_{h2h2} = 25, a_{t2t2} = 25, a_{h1t1} = 100, a_{h1s} = 25, a_{t1s} = 100, a_{h2t2} = 100, a_{h2s} = 25, a_{t2s} = 100, a_{h1T} = 25, a_{t1T} = 100, a_{h2T} = 25, a_{t2T} = 100, a_{h1t2} = 100, a_{h2t1} = 100 \text{ and } a_{h1h2} = 25.$$

Where ‘s’ represents solvent, ‘h’ represents head, ‘t’ represents tail, ‘T’ represents tether, ‘1’ and ‘2’ represent lipid type. The values of the inter-specie tail-tail soft repulsive interaction parameter  $a_{t1t2}$  will span values ranging from 31 to 50, to mimic mixtures of amphiphilic species with different tail group properties.

### 3.2.2 Role of Confinement

The system components are modeled similar to bulk conditions, exception being that tethers are modeled by three, five and six hydrophilic beads, which experimentally correspond to 6, 10 and 12 degree of polymerization (n). Two planar walls, each consisting of frozen DPD particles with thickness of  $0.85r_c$  and a total area of  $1779r_c^2$  are placed along the xy-plane as shown in Figure 3.2 (a). Wall beads are organized in a triangular lattice. The walls are modeled in such a way that they have favorable interactions with the solvent molecules and unfavorable interactions with the amphiphilic species. A hydrophilic surface with a charge distribution resulting in unfavorable enthalpic interactions with amphiphilic molecules can be a relevant experimental counterpart<sup>100</sup> for the modeled planar walls. Microfluidic channels sealed with oxidized poly(dimethylsiloxane) (PDMS) are found to be negatively charged in neutral and basic

aqueous solutions<sup>101</sup>. It has been previously shown that vesicles composed of neutral and negatively charged lipid molecules, such as DOPC/DOPS, are not adsorbing onto the negatively charged silica surface<sup>102</sup>.

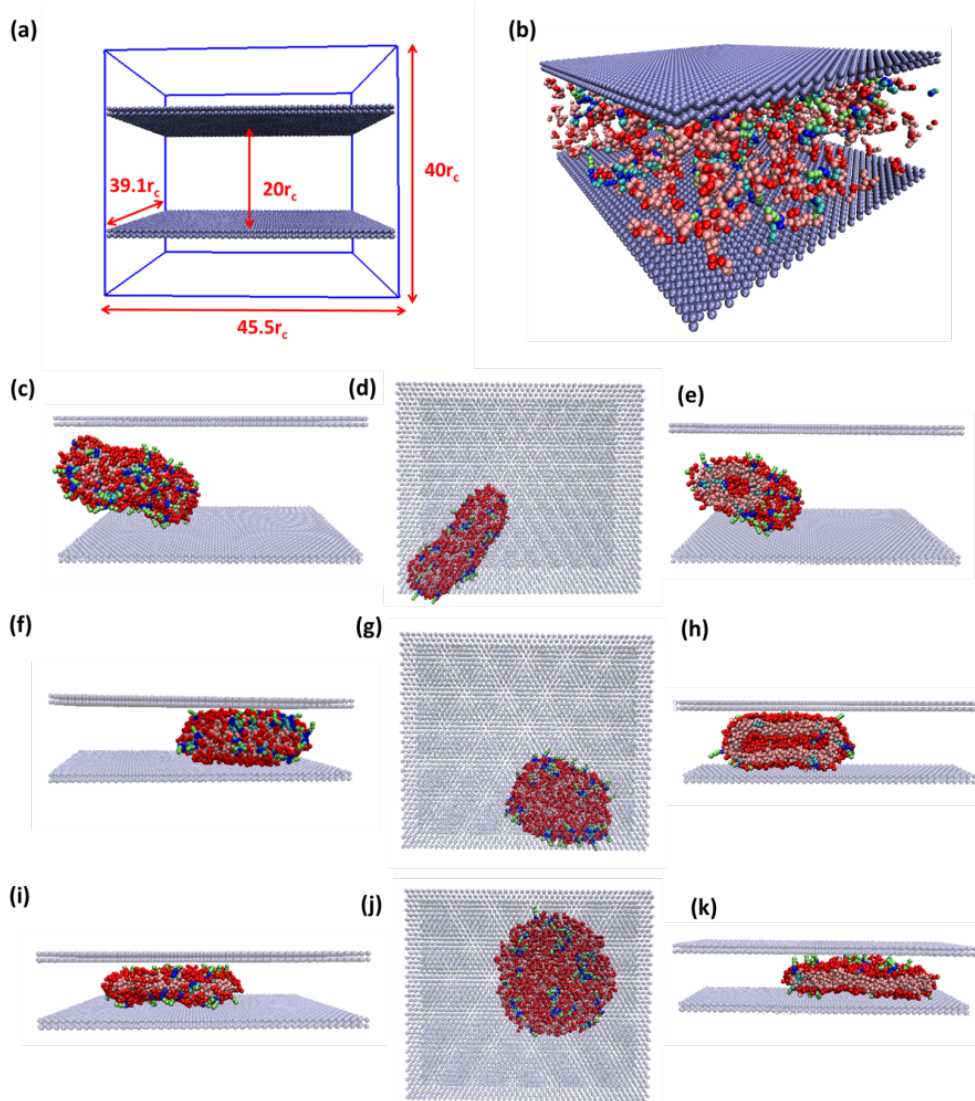


Figure 3.2: (a) The dimensions of the three-dimensional simulation box and channel used to confine the amphiphilic molecules. (b) The initial system configuration for a mixture of phospholipid and hairy lipid molecules in the confinement with a channel height of  $15r_c$ . (c) A side, (d) top and (e) cross-sectional view of a self-assembled prolate vesicle in the

confinement with a channel height of  $20r_c$  at time  $t = 120,000\tau$ . (f) A side, (g) top and (h) cross-sectional view of a self-assembled oblate vesicle in the confinement with a channel height of  $10r_c$  at time  $t = 120,000\tau$ . (i) A side, (j) top and (k) cross-sectional view of a self-assembled bicelle in the confinement with a channel height of  $8r_c$  at time  $t = 120,000\tau$ . The systems in (b) – (k) are composed of phospholipids (90%) and hairy lipid molecules with tethers composed of three beads (10%). The wall beads are reduced in size to enhance the top view of the different vesicle morphologies.

The soft repulsive pair potential parameters between different species are assigned the following values in order to capture the amphiphilic nature of species. The units for the parameters are  $k_B T / r_c$ .

$$a_{ss} = 25, a_{TT} = 25, a_{Ts} = 25, a_{h1h1} = 25, a_{t1t1} = 25, a_{h2h2} = 25, a_{t2t2} = 25, a_{h1t1} = 100, a_{h1s} = 25, a_{t1s} = 100, a_{h2t2} = 100, a_{h2s} = 25, a_{t2s} = 100, a_{h1T} = 25, a_{t1T} = 100, a_{h2T} = 25, a_{t2T} = 100, a_{h1t2} = 100, a_{h2t1} = 100, a_{h1h2} = 25, a_{sw} = 25, a_{Tw} = 100, a_{h1w} = 100, a_{h2w} = 100, a_{t1w} = 100 \text{ and } a_{t2w} = 100.$$

Where ‘s’ represents solvent, ‘h’ represents head, ‘t’ represents tail, ‘T’ represents tether, ‘w’ represents wall, ‘1’ and ‘2’ represent lipid type.

### 3.3 Results and Discussions

#### 3.3.1 Aggregation dynamics influenced by intrinsic factors

Initially, phospholipids and short tether hairy lipids in a 9:1 ratio are placed in random positions in a solvent, in a simulation box of  $30 \times 30 \times 30 r_c^3$ . The amphiphilic species i.e., the phospholipids and hairy lipids constitute to 5.6% of the total number beads in the simulation box. The simulation capturing the unfavorable enthalpic

interactions between hydrophilic and hydrophobic species is run for a time interval of  $60,000\tau$ . The self-assembly process is fundamentally, an interplay between the minimization of the unfavorable enthalpic interactions and maximization of the molecular configurational<sup>103</sup> and conformational entropy. The self-assembly process begins with diffusion, collision, coalescence of lipid molecules forming small clusters and continues with the formed clusters diffusing, colliding, coalescing to form larger clusters and so on. A cluster is a group of non-solvent beads whose center-to center distance is within their interaction cut-off range which is given by  $r_c=1$ . In this chapter, we study how intrinsic factors like tether length and relative concentration of hairy lipids influence the aggregation dynamics. The relative concentrations of the hairy lipids studied in this chapter are 10%, 20%, 30%, 40% and 50% for short tethers, and 10% and 20% for long tethers. The simulations are run for 16 random seeds with identical initial conditions.

One of the factors listed above that influence the equilibrium morphology of the vesicle is the increase in steric effect, which is a direct result of high relative concentration of the hairy lipids. Experimental<sup>32</sup> and theoretical<sup>95</sup> studies predict have demonstrated that average cluster size decreases with the increase in relative concentration of grafted tethers because of the increased repulsive forces over the vesicle surface due to grafted tethers. Average cluster size is defined as the sum of the number of phospholipid and hairy lipid molecules divided by the total number of clusters. We also predict based on our scaling exponent data, that the growth dynamics of the aggregates decelerates with increased relative concentration of grafted tethers and tether length. The time evolution of the aggregates during self-assembly is characterized using scaling exponents. We calculate

scaling exponents based on the number of clusters and average size of clusters using following equations

$$N(t) \sim C t^{-\alpha} \quad (3.1)$$

where  $N(t)$  is the number of clusters,  $C$  is a constant,  $t$  is time and  $\alpha$  is the scaling exponent. Similarly, the growth in the average size of a cluster can be characterized using

$$\langle S(t) \rangle \sim D t^{\beta} \quad (3.2)$$

where  $\langle S(t) \rangle$  is the average cluster size,  $D$  is a constant,  $t$  is time, and  $\beta$  is the scaling exponent. The scaling exponent results are as shown in Table 3.1.

<b>Tether length = 3</b>		
<b>Concentrations (%)</b>	<b>Scaling Exponent (<math>\alpha</math>)</b>	<b>Scaling Exponent (<math>\beta</math>)</b>
10	-0.84±0.07	0.85±0.07
20	-0.81±0.07	0.81±0.07
30	-0.78±0.04	0.78±0.04
40	-0.77±0.09	0.78±0.09
50	-0.75±0.05	0.76±0.06
<b>Tether length = 6</b>		
10	-0.80±0.07	0.81±0.07
20	-0.77±0.08	0.78±0.08

Table 3.1: Table of the scaling exponents  $\alpha$  and  $\beta$  for the self-assembly of binary mixtures composed of different relative concentrations of hairy lipid and phospholipid molecules, and length of the tethers.

The slower growth dynamics may have been observed due to the higher drag forces experienced by the lipid molecules because of the favorable enthalpic interaction of the grafted tethers with solvent molecules.<sup>104,105</sup> Our results are in good agreement with aggregation dynamics of phospholipid molecules and hairy nanotubes.<sup>41</sup> The time evolution of the aggregation dynamics is as shown in Figure 3.3.

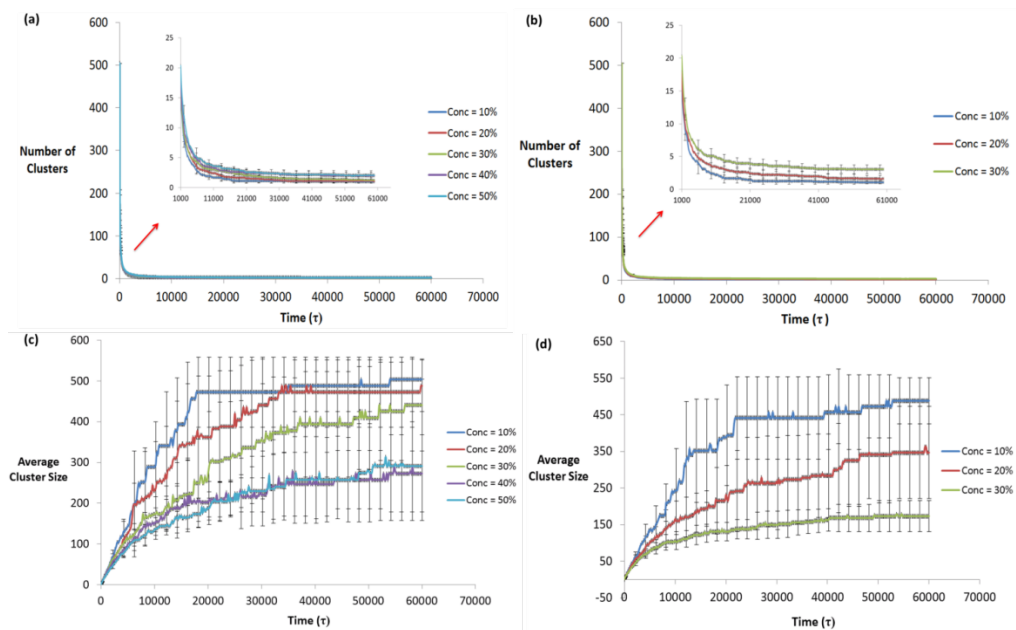


Figure 3.3: The time evolution (beginning from time  $t = 1,000\tau$ ) of the total number of clusters encompassing mixtures of phospholipids and hairy lipids with tethers composed of (a) three beads, for relative concentration of the hairy lipids given by 10%, 20%, 30%, 40% and 50%, and (b) six beads, for relative concentration of the hairy lipids given by 10% and 20%. The inset in (a) and (b) show the time evolution of the total number of clusters between the time interval  $t = 0$  and  $t = 1,000\tau$ . (c) The time evolution for the

*average cluster size for mixtures of phospholipids and hairy lipid molecules with the tethers composed of (c) three beads, for relative concentration of the hairy lipids given by 10%, 20%, 30%, 40% and 50%, and (d) six beads, for relative concentration of the hairy lipid given by 10% and 20%.*

### **3.3.2 Aggregation dynamics influenced by extrinsic factors**

In this part of the chapter, we study the effect of confinement over the aggregation dynamics of phospholipids and hairy lipids. For this purpose, we place the lipids in a confined volume bound by rectangular planes, which act as repellant walls. The simulation box has dimensions of  $45.4 \times 39.1 \times 40r_c^3$  with periodic boundaries along all three directions. The walls are equidistant from the origin of the simulation box over the z-axis as shown in Fig 3.2(a). To study the aggregation dynamics under different degrees of confinement, the distance between the wall planes is varied from  $8r_c$  to  $20r_c$ . The system consists of 504 lipid molecules with three different relative concentrations of phospholipid to hairy lipids, i.e., 8:2 (20% hairy lipids), 8.5:1.5 (15% hairy lipids) and 9:1 (10% hairy lipids). Three different tether lengths of 3, 5, 6 beads have been used. The molecules are placed randomly between the two walls with solvent present between and beyond the walls as shown in Fig 3.2(b). The simulations are run for a time interval of  $120,000\tau$ . Similar to the case without any confinement, initially small clusters are formed which subsequently aggregate to form larger clusters by diffusion, collision and coalescence. The aggregation dynamics under confinement are characterized by calculating the scaling exponents for three different tether lengths of 3, 5, 6 beads for 10%, 15%, 20% relative concentrations of hairy lipids. The degree of confinement is varied by setting channel width at  $8r_c$ ,  $10r_c$ ,  $15r_c$ ,  $20r_c$  along the z axis. The simulations

are run for 4 different random seeds with same initial conditions. The scaling exponents calculated are as shown in Figure 3.4.

No significant difference is observed for scaling exponents calculated at channel widths of  $15r_c$  and  $20r_c$ . Scaling exponents are also calculated for self-assembly in bulk conditions and the results obtained are within 2-5% of the scaling exponents calculated for channel width of  $20r_c$ . This indicates that the effect of confinement is negligible for channel width of  $20r_c$ . This indicates that the effect of confinement is negligible for channel heights of  $15r_c$  and  $20r_c$ . Thus, we conclude from Figure 3.4 that decrease in channel width leads to deceleration of aggregation dynamics. We expect that the aggregation decelerates due to increase in tether length as observed in the case of self-assembly in bulk conditions. We observe concurrent results when the channel width is  $15r_c$  and  $20r_c$ , but the effect of tether length is not observed at higher degree of confinement. Also, the relative concentration of the hairy lipids also ceases to show any effect on the aggregation dynamics.

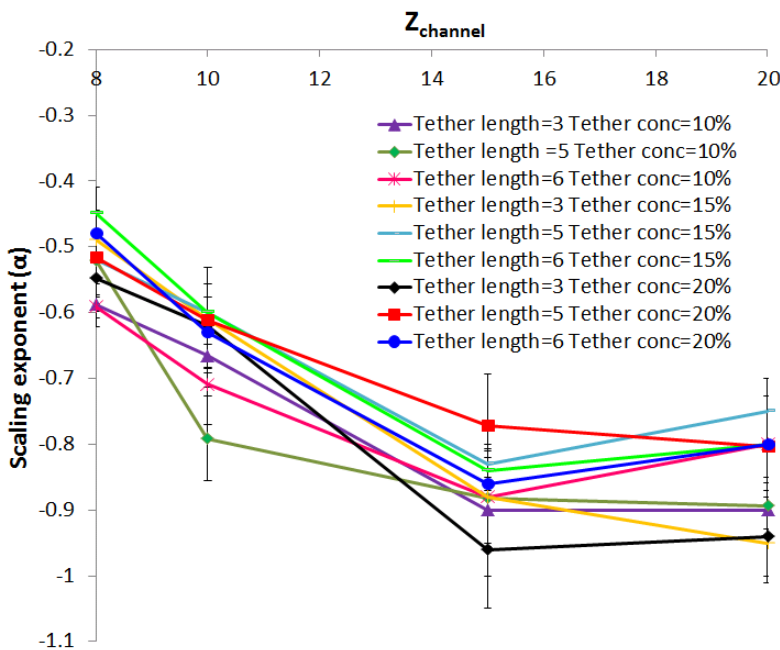


*Figure 3.4: A plot of the scaling exponent  $\alpha$  as a function of the distance between two planar surfaces for the self-assembly of binary mixtures composed of different relative concentrations of hairy lipid and phospholipid molecules, and length of the tethers.*

### 3.3.3 Tether distribution

After studying the aggregation dynamics of the system, we extend our investigations to understand the organization of species within the vesicle. The vesicle can be divided into two subparts namely inner and outer monolayers. The inner monolayer has tightly packed molecules due to its smaller volume compared to the outer monolayer. For the same reason, tethers with similar excluded volume are expected to be present more on the outer monolayer compared to inner monolayer. The excluded volume of a tether is measured through radius of gyration. The radius of gyration can be calculated using the following equation

$$R_g^2 = \frac{[\sum_{i=1, N+1} (\mathbf{r}_i - \mathbf{r}_{cm})^2]}{(N + 1)} \quad (3.3)$$

where  $\mathbf{r}_i$  is the position vector for each tether bead,  $\mathbf{r}_{cm}$  is the position vector for center-of-mass of a tether and  $N$  is the number of beads per tether. Radius of gyration of each tether in a given monolayer is calculated and averaged over all the tethers post equilibration. The organization of species between two monolayers is well described by Table 3.2.

	Conc. (%)	Number of Hairy Lipids in the Inner Monolayer	Number of Hairy Lipids In the Outer Monolayer	Radius of Gyration in the Inner Monolayer ( $r_c$ )	Radius of Gyration In the Outer Monolayer ( $r_c$ )	Minimum Radius ( $r_c$ )	Maximum Radius ( $r_c$ )
Tether length = 3	10	10	40	$0.37 \pm 0.02$	$0.37 \pm 0.02$	$4.3 \pm 0.2$	$10.7 \pm 0.5$
	20	11	90	$0.36 \pm 0.02$	$0.36 \pm 0.02$	$3.8 \pm 0.3$	$11.8 \pm 0.4$
	30	15	137	$0.36 \pm 0.01$	$0.36 \pm 0.01$	$4.0 \pm 0.2$	$11.3 \pm 0.3$
	40	39	163	$0.37 \pm 0.01$	$0.37 \pm 0.01$	$4.2 \pm 0.01$	$11.1 \pm 0.3$
	50	50	202	$0.37 \pm 0.01$	$0.37 \pm 0.01$	$4.7 \pm 0.2$	$10.3 \pm 0.3$
Tether	10	6	44	$0.56 \pm 0.04$	$0.56 \pm 0.04$	$4.1 \pm 0.2$	$11.3 \pm 0.4$
	20	4	97	$0.54 \pm 0.03$	$0.54 \pm 0.03$	$4.1 \pm 0.2$	$11.3 \pm 0.3$

Table 3.2: The number of hairy lipid molecules and the radius of gyration of the tethers present in the inner and outer monolayers of the self-assembled vesicles, and maximum and minimum distances from the center of mass of the vesicle to the lipid head groups in the outer monolayer for different relative concentrations of the hairy lipids and tether lengths.

An unbalanced distribution of tethers, where the inner shell has less number of tethers is observed. This could be because of the smaller volume of the inner monolayer not being to accommodate the excluded volume of the tethers. The disproportion in tether distribution is more pronounced in the case of longer tethers compared to their shorter counter parts, contributing towards the validity of the hypothesis made. A similar hypothesis can be made for the difference in the radius of gyration of the tethers

distributed across the monolayers. We note that the radius of gyration for the longer tethers is higher in the outer monolayer than the inner monolayer. We surmise that the tethers pack themselves into the inner monolayer shell reducing their excluded volume. Our observations are in good agreement with experimental<sup>31</sup> and theoretical<sup>33,95</sup> studies which demonstrated the disproportionate distribution of molecular species between two monolayers due to tightly packed inner region of aggregates of amphiphilic molecules. The radius of gyration and tether distribution are not found to be affected by confinement as shown in Table 3.3 and Table 3.4

	Conc. (%)	Radius of gyration in the inner monolayer ( $r_c$ )	Radius of gyration in the outer monolayer ( $r_c$ )
<b>Tether length = 3</b> <b>Z<sub>channel</sub> = 10r<sub>c</sub></b>	10	0.43±0.01	0.43±0.02
	15	0.41±0.02	0.42±0.01
	20	0.42±0.01	0.44±0.02
<b>Tether length = 5</b> <b>Z<sub>channel</sub> = 10r<sub>c</sub></b>	10	0.59±0.06	0.72±0.02
	15	0.59±0.06	0.73±0.02
	20	0.58±0.04	0.74±0.02
<b>Tether length = 6</b> <b>Z<sub>channel</sub> = 10r<sub>c</sub></b>	10	0.73±0.07	0.89±0.03
	15	0.72±0.07	0.87±0.03
<b>Tether length = 3</b> <b>Z<sub>channel</sub> = 15r<sub>c</sub></b>	10	0.40±0.03	0.41±0.02
	15	0.40±0.03	0.43±0.01
	20	0.42±0.02	0.42±0.01
<b>Tether length = 5</b> <b>Z<sub>channel</sub> = 15r<sub>c</sub></b>	10	0.63±0.04	0.71±0.03
	15	0.61±0.04	0.70±0.03
	20	0.64±0.04	0.71±0.02
<b>Tether length = 6</b> <b>Z<sub>channel</sub> = 15r<sub>c</sub></b>	10	0.74±0.06	0.84±0.04
	15	0.71±0.05	0.87±0.02
	20	0.74±0.04	0.84±0.04
<b>Tether length = 3</b> <b>Z<sub>channel</sub> = 20r<sub>c</sub></b>	10	0.40±0.01	0.43±0.01
	15	0.41±0.02	0.43±0.01
	20	0.40±0.01	0.42±0.01
<b>Tether length = 5</b> <b>Z<sub>channel</sub> = 20r<sub>c</sub></b>	10	0.64±0.05	0.71±0.03
	15	0.61±0.03	0.70±0.01
	20	0.64±0.04	0.70±0.02
<b>Tether length = 6</b> <b>Z<sub>channel</sub> = 20r<sub>c</sub></b>	10	0.78±0.04	0.83±0.02
	15	0.72±0.05	0.85±0.04
	20	0.72±0.05	0.84±0.02

*Table 3.3: The radius of gyration of the tethers presents in the inner and outer monolayers of the self-assembled vesicles for different relative concentrations of the*

*hairy lipids and tether lengths in the confinement with a channel height of  $10r_c$ ,  $15r_c$  and  $20r_c$ .*

	Conc. (%)	Number of tethers in the inner monolayer	Number of tethers in the outer monolayer
Tether length = 3 $Z_{\text{channel}} = 10r_c$	10	7±1	43±1
	15	12±4	64±4
	20	17±1	84±1
Tether length = 5 $Z_{\text{channel}} = 10r_c$	10	6	44
	15	6±1	70±1
	20	7	94
Tether length = 6 $Z_{\text{channel}} = 10r_c$	10	5	45
	15	4	72
Tether length = 3 $Z_{\text{channel}} = 15r_c$	10	5±1	45±1
	15	11±2	65±2
	20	14±2	87±2
Tether length = 5 $Z_{\text{channel}} = 15r_c$	10	4±1	46±1
	15	7±3	69±3
	20	9±1	92±1
Tether length = 6 $Z_{\text{channel}} = 15r_c$	10	2±1	48±1
	15	5±2	71±2
	20	4±1	97±1
Tether length = 3 $Z_{\text{channel}} = 20r_c$	10	9±1	41±1
	15	10±2	66±2
	20	17±1	84±1
Tether length = 5 $Z_{\text{channel}} = 20r_c$	10	5±1	45±1
	15	5±2	71±2
	20	9±2	92±2
Tether length = 6 $Z_{\text{channel}} = 20r_c$	10	3±1	47±1
	15	8	68
	20	7±1	94±1

*Table 3.4: The number of hairy lipid molecules present in the inner and outer monolayers of the self-assembled vesicles for different relative concentrations of the hairy lipids and tether lengths at different degrees of confinement.*

### 3.3.4 Morphology influenced by intrinsic factors

We classify the morphology of a vesicle as ellipsoidal and spherical based on the minimum and maximum distances from the vesicle's center of mass to the lipid head group in the outer monolayer. The vesicles with a large difference between minimum and maximum distance are termed ellipsoidal and the opposite are termed spherical. We

study, molecular stiffness of a species, spatial distribution of one species in bilayers, specifically where one of the species has a curvature inducing functional group<sup>38-40</sup>, as intrinsic factors which can affect the morphology of the vesicle with different relative concentration of hairy lipids and tether lengths. The stiffness of the chains is varied by varying their angle potential constants ( $K_{\text{angle}}$ ). The angle potential constant of the hairy lipid is set to 0, while that for the phospholipid is varied from 5-20. An experimental example for a saturated lipid molecular species with stiffer tails is 1,2-distearoyl-sn-glycero-3-phosphocholine with 18 carbon atoms in each hydrocarbon chain<sup>106</sup>, where as DPPC is a saturated phospholipid with 16 carbon atoms in each hydrocarbon tail. The simulations are run over a time interval of  $5000\tau$  using different values of  $K_{\text{angle}}$  for phospholipid species. We expect that higher chain stiffness would lead to a tighter packing of the molecules at lower tether concentrations, hence resulting in a more spherical structure. At higher tether concentration the excluded volume of tethers becomes more prominent and reduces the effect of chain stiffness over the morphology. Higher excluded volume of tethers hence would result in an ellipsoidal morphology. These predictions are validated by the results compiled in Figure 3.5.

To develop a systematic parameterization of the shape transformation of the hairy vesicle, we have examined the role of factors such as the concentration of the hairy lipids ( $x_{\text{tether}}$ ) and the molecular stiffness of the phospholipid tails ( $K_{\text{angle}}$ ) on the interfacial line tension, the ratio of minimum to maximum distance of the head groups in the outer monolayer from the center of mass of the hairy vesicle ( $r_{\text{min}}/r_{\text{max}}$ ), and the reduced volume<sup>107</sup> ( $v$ ). We summarize our results in phase diagrams, as shown in Figure 3.6.

Tether Length	Relative Concentration of Tethers (%)	$K_{angle}$			
		5	10	15	20
Tether length of 3	10				
	20				
	30				
	40				
	50				
Tether length of 6	10				
	20				

Figure 3.5: Equilibrium configurations of the binary hairy vesicle composed of a range of concentrations of the hairy lipids (10% to 50% for the short tethers and 10% to 20% for the long tethers) at  $t = 5,000\tau$ , for different hydrocarbon chain stiffness of the phospholipid specie given by  $K_{angle} = 5, 10, 15,$  and  $20$ . The angle coefficient of the hairy lipid hydrocarbon chain was set at  $K_{angle} = 0$ .

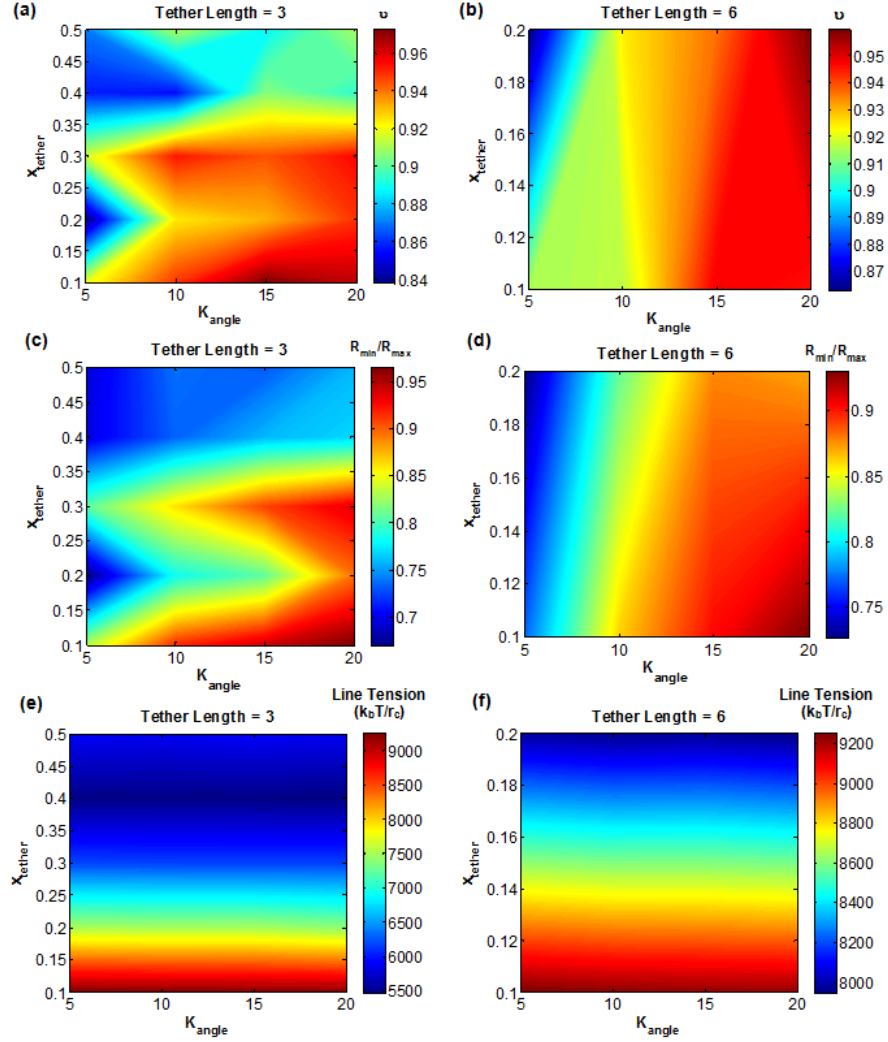


Figure 3.6: The phase diagram for the reduced volume of the self-assembled hairy vesicles with tethers composed of (a) three beads, (b) six beads as a function of  $x_{tether}$  and  $K_{angle}$ . The phase diagram for the  $r_{min}/r_{max}$  of the self-assembled hairy vesicles with tethers composed of (c) three beads, (d) six beads as a function of  $x_{tether}$  and  $K_{angle}$ . The phase diagram for the interfacial line tension of the self-assembled hairy vesicles with tethers composed of (e) three beads, (f) six beads as a function of  $x_{tether}$  and  $K_{angle}$ .  $x_{tether}$  is varied from 0.1 to 0.5 for lipid species with short tethers and from 0.1 to 0.2 for lipid species with long tethers.  $K_{angle}$  for the phospholipids is varied from 5 to 20.

In Figure 3.6 (a) and Figure 3.6 (b) we observe that at lower concentrations of the hairy lipids, the reduced volume approaches to 1.0 indicating a more spherical morphology. This result is in concurrence with our observations in Figure 3.6. Similar trends are observed for  $r_{\min}/r_{\max}$  in Figure 3.6(c) and 3.6(d). Our results demonstrate that equilibrium morphology of binary hairy vesicles is determined by an interplay between packaging of the molecular species and the excluded volume of the curvature-inducing species. The shape changes with molecular stiffness are observed to be independent of tether length.

We estimate line tension using the following equation<sup>108</sup>

$$\lambda \equiv \frac{1}{2} (U_{AA} + U_{BB}) - U_{AB} / l_{mo} \quad (3.4)$$

where  $U_{AA}$ ,  $U_{BB}$ ,  $U_{AB}$  are the pair interaction energies between components A and B and  $l_{mo}$  is the lateral size of the lipid molecules. We observe the line tension to decrease with higher relative concentrations of the hairy lipids. We surmise that this may be because of the reduced interactions between neighboring hairy lipids due to excluded volume of tethers. Similar observations were made by an earlier computational study<sup>109</sup> for a bicellar structure composed of a mixture of zwitterionic and PEGylated lipid molecules.

The influence of spatial distribution of species over morphology can be studied by using conditions that promote macroscopic phase segregation<sup>40</sup> in the bilayer. We investigate the phase segregation within the bilayer of a hairy vesicle composed of phospholipids and hairy lipids in a 1:1 ratio with distinct hydrophobic tail groups. The distinction in the tail groups is effectively captured by tail-tail interaction parameter  $a_{t1t2}$ . The range of tail-tail interaction parameters used in this study for inducing macroscopic

phase segregation is 31-50. The simulations are run over a time interval of  $1000\tau$ . The simulations are run for 4 different random seeds with same initial conditions.

To demonstrate that the latter dynamics of the phase separation process is determined by the evaporation-condensation effect<sup>2,110</sup>, we measure the scaling exponents of the time evolution of the number of clusters ( $\alpha$ ) and the average cluster size ( $\beta$ ) as shown in Figure 3.7. In this case a cluster is defined as a domain of hairy lipid molecules whose head group beads are within interaction range from each other. From our results in Table 3.5 we observe that there is an accelerated cluster growth when the dissimilarity between the hydrocarbon chains is high and the tethers are short. We surmise that this is because of less drag experienced by shorter tethers compared to longer ones.

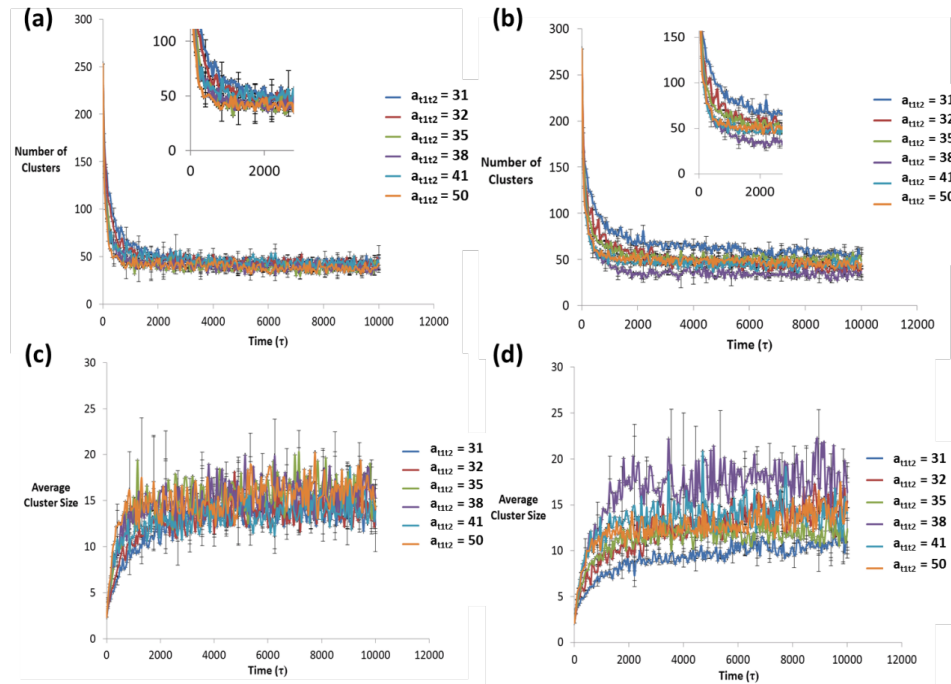


Figure 3.7: A plot of the time evolution of the total number of clusters of the hairy lipid molecules with (a) short and (b) long tethers. A plot of the time evolution for the average size of the clusters composed of hairy lipids with (c) short and (d) long tethers. All the

simulations start from a completely mixed state. The inter-specie tail-tail soft repulsive interaction parameter was set at the following values:  $a_{112} = 31, 32, 35, 38, 41, \text{ and } 50$ .

$a_{ij}$ ( $k_b T/r_c$ )	Scaling Exponent ( $\alpha$ )	Scaling Exponent ( $\beta$ )
<b>Tether length = 3</b>		
31	-0.45	0.46
32	-0.50	0.50
35	-0.50	0.52
38	-0.51	0.52
41	-0.51	0.48
<b>Tether length = 6</b>		
31	-0.33	0.34
32	-0.33	0.34
35	-0.36	0.37
38	-0.46	0.46
41	-0.47	0.48
50	-0.47	0.48

Table 3.5: Table of the scaling exponents  $\alpha$  and  $\beta$  for the coarsening dynamics in the bilayer of a binary hairy vesicle induced by the dissimilarity of the hydrocarbon tail groups of the phospholipid and hairy lipids, for different tether lengths.

From our calculations we find that the area per lipid increases by 30% for hairy lipid with short hairs and 50% for hairy lipids with long hairs compared to area per phospholipid calculated to be  $1.12 r_c^2$  as shown in Table 3.6. This kind of increase has been previously observed by experimental<sup>96</sup> and computational<sup>109</sup> studies.

	$a_{t1t2}$ ( $k_b T/r_c$ )	Area Per Hairy Lipid Molecule in the Inner Monolayer ( $r_c^2$ )	Area Per Hairy Lipid Molecule In the Outer Monolayer ( $r_c^2$ )
Tether length = 3	31	1.2±0.1	1.7±0.1
	32	1.2±0.1	1.8±0.1
	35	1.3±0.1	1.8±0.2
	38	1.2±0.1	1.8±0.2
	41	1.3±0.2	1.8±0.2
	50	1.3±0.2	1.8±0.2
Tether length = 6	31	1.5±0.1	2.0±0.1
	32	1.4±0.2	1.9±0.1
	35	1.5±0.1	2.0±0.1
	38	1.4±0.1	1.9±0.1
	41	1.5±0.2	2.0±0.2
	50	1.5±0.2	2.0±0.2

Table 3.6: The area per hairy lipid for tethers composed of three and six beads in the inner and outer monolayers of the binary hairy vesicle as a function of the inter-specie tail-tail soft repulsive interaction parameters  $a_{t1t2}$ .

We characterize shape change by minimum and maximum radius of the vesicle as shown in Figure 3.8 (e). We observe the transition of shape from spherical to ellipsoidal

with increase in distinction between tail groups. Morphological changes of vesicles composed of various amphiphilic species can be related to interfacial line tension. Figure 3.8 (f) represents line tension measurements performed on particle trajectories beginning from  $10,000\tau$  until  $15,000\tau$ . Each data point has been averaged over time and total number of beads in the system. The line tension is observed to increase with tether length and tail dissimilarity and in turn affects the shape of phase segregated vesicle.

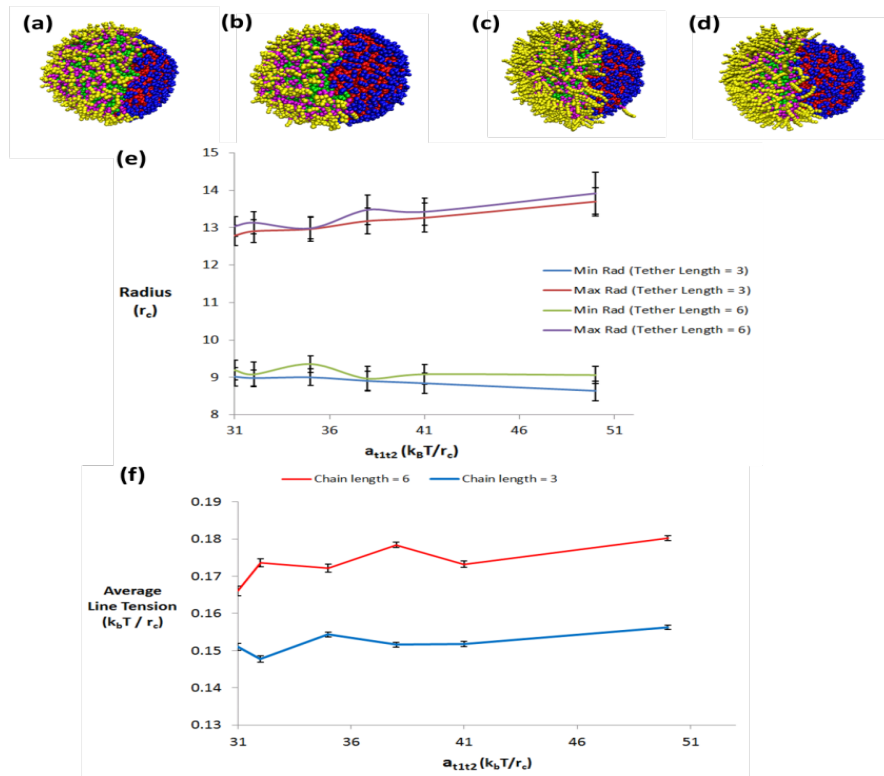


Figure 3.8: Final configurations of the binary hairy vesicle at time  $t = 10,000\tau$  for different soft repulsive interaction parameters between the tail groups of the phospholipids and hairy lipids given by (a)  $a_{t1t2} = 31$ , (b)  $a_{t1t2} = 50$ , and (c)  $a_{t1t2} = 31$ , (d)  $a_{t1t2} = 50$ , respectively for short and long tethers. Plots of the (e) minimum and maximum distance of the lipid head beads from the COM of vesicle, and (f) average line tension as function of  $a_{t1t2}$ .

### 3.3.5 Morphology influenced by extrinsic factors

In this section, we explore the effect of confinement over the shape of vesicle. We characterize shape by measuring the reduced volume ( $v$ ) of hairy vesicles. The reduced volume for any structure ranges between 0-1, where 1 indicates spherical morphology. Our measurements as shown in Figure 3.9 show that vesicles assume a prolate (cigar shaped), oblate (disk shaped) or bicelle morphology depending on the degree of confinement. The aggregates tend to form a prolate structure with reduced volume in the range of 0.7-0.8, when simulations are run with planar distance set at  $15r_c$  or  $20r_c$  as shown in Figure 3.2 (c) to Figure 3.2 (e). The reduced volumes obtained for aforementioned degrees of confinement are similar to that measured in bulk conditions as shown in Table 3.7.

We repeat the simulations by reducing the planar distance to  $10r_c$ . We find that the vesicle tends to assume oblate morphology as shown in Figure 3.2 (f) – 3.2 (h), with reduced volume in range of 0.8-0.9, with a slight increase in degree of confinement.

We conclude from this observation that there is a transition from prolate to oblate morphology with increase in degree of confinement.

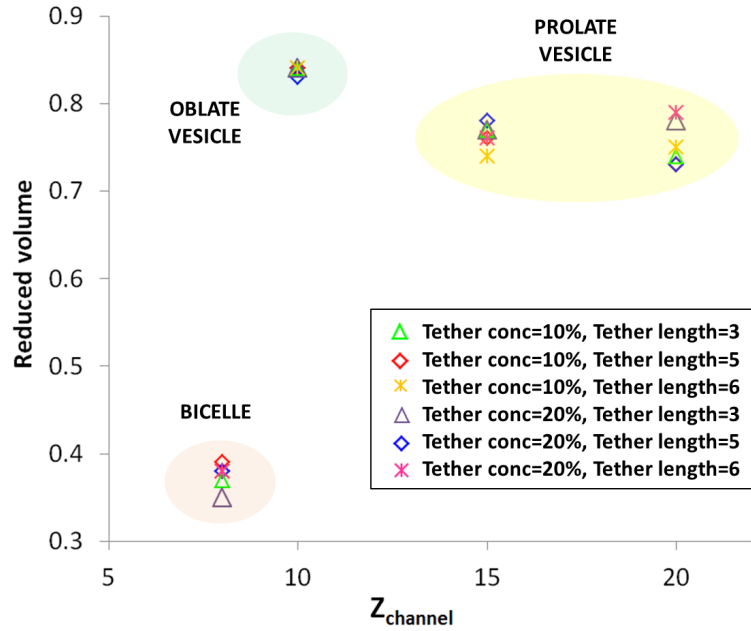


Figure 3.9: A plot of the reduced volume of the self-assembled hairy vesicles as a function of the distance between two planar surfaces for different relative concentrations of the hairy lipids and tether lengths.

	Conc. (%)	Reduced volume ( $v$ )	x-axis ( $r_c$ )	y-axis ( $r_c$ )	z-axis ( $r_c$ )
Tether length = 3 No wall	10	$0.76 \pm 0.05$	$16 \pm 2$	$5.5 \pm 0.5$	$4.5 \pm 0.3$
	15	$0.74 \pm 0.03$	$16 \pm 1$	$5.5 \pm 0.5$	$4.4 \pm 0.2$
	20	$0.81 \pm 0.07$	$14 \pm 3$	$6 \pm 1$	$4.6 \pm 0.3$
Tether length = 5 No wall	10	$0.75 \pm 0.06$	$17 \pm 2$	$5.5 \pm 0.6$	$4.3 \pm 0.3$
Tether length = 6 No wall	10	$0.75 \pm 0.06$	$16 \pm 2$	$5.6 \pm 0.6$	$4.4 \pm 0.4$

Table 3.7: The reduced volume and the x, y, z - principal axes of the self-assembled hairy vesicles for different relative concentrations of the hairy lipids and tether lengths in bulk conditions (without walls).

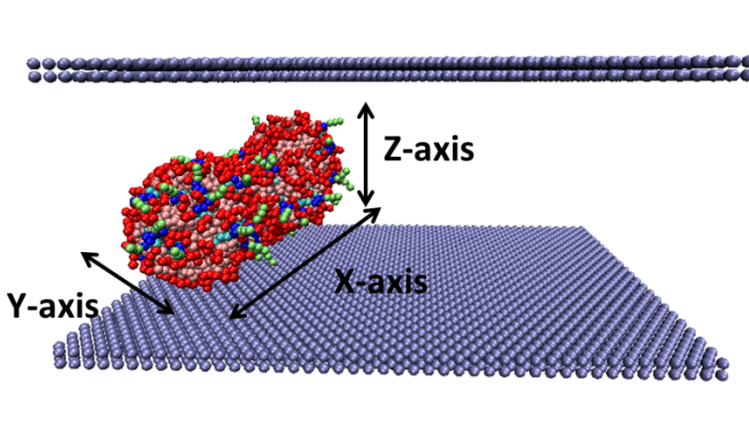
We surmise that for cases with very low degree of confinement, the prolate shape of the vesicle allows the aggregate to maximize its rotational entropy about its principal axes parallel or perpendicular to planar walls. In case with higher degree of confinement, the aggregate maximizes its rotational entropy to be able to rotate about its principal axis perpendicular to the wall by assuming oblate shape. A theoretical study<sup>111</sup> conducted by Helal et al. via the use of Area Difference Elasticity (ADE) model discussed the shape transition from prolate to oblate morphology. Our findings for reduced volumes of prolate morphology are in good agreement with their findings. However, their findings for oblate vesicles are contrary to our findings. They find that  $v_{\text{oblate}} < 0.65$ , which is clearly not our case. This might be due to the fact that the self-assembly of vesicles, under the confinement, did not preserve the total volume or area of the membrane on account of the inter-monolayer asymmetric distribution of the hairy lipids, as shown in

Table 3.8.

	Conc. (%)	Surface area ( $r_c^2$ )	Enclosed volume ( $r_c^3$ )
<b>Tether length = 3</b> $Z_{\text{channel}} = 10r_c$	10	690±7	1430±10
	20	694±9	1440±20
<b>Tether length = 3</b> $Z_{\text{channel}} = 15r_c$	10	730±20	1500±40
	20	760±30	1530±50
<b>Tether length = 3</b> $Z_{\text{channel}} = 20r_c$	10	800±40	1590±60
	20	760±30	1530±50
<b>Tether length = 3</b> <b>Without walls</b>	10	790±30	1570±60
	20	780±30	1580±50
<b>Tether length = 6</b> $Z_{\text{channel}} = 10r_c$	10	700±10	1440±20
<b>Tether length = 6</b> $Z_{\text{channel}} = 15r_c$	10	810±30	1560±60
	20	780±30	1550±50
<b>Tether length = 6</b> $Z_{\text{channel}} = 20r_c$	10	790±40	1570±50
	20	750±30	1530±50
<b>Tether length = 6</b> <b>Without walls</b>	10	830±30	1640±60

*Table 3.8: The total outer surface area and enclosed volume of the self-assembled hairy vesicles for different relative concentrations of the hairy lipids and tether lengths at different degrees of confinement.*

We would like to note that Helal et al.<sup>111</sup> use preconfigured vesicle shapes, and fixed enclosed volume and total area of the membrane. Also, they do not include the thermal fluctuations of the bilayer in their model. Simulations are run again with even higher degree of confinement with planar distance set at  $8r_c$ . These simulations result in a bicellar morphology with reduced volumes in range of 0.3-0.4, as shown in Figure 3.2 (i) – 3.2 (k). Along with reduced volume, vesicle morphology can also be characterized by measurement of principal axes<sup>112</sup> of the equilibrated aggregates as shown in Figure 3.10.



*Figure 3.10: An image that shows the principal axes ( $x$ ,  $y$  and  $z$ ) of the self-assembled binary hairy vesicle with a prolate morphology.*

In order to find the principal axes, the algebraic expression of the ellipsoid is formed in the matrix of the quadratic form. The ellipsoid is centered in the Cartesian coordinate system by first finding its center and then forming its corresponding translation matrix. The translation matrix can be used to determine the principal axes by

solving the eigenvalue problem. We measure the principal axes for different relative concentration of hairy lipids, tether length and degree of confinement. The results for bulk and confined conditions are tabulated in Table 3.7 and 3.9 respectively. These observations are consistent with the observations made when reduced volume was calculated. The vesicle is observed to assume prolate morphology when the distance between the walls is  $15r_c$  and  $20r_c$ , oblate shape when the distance between the walls is  $10r_c$ , bicellar structure when distance between the walls is  $8r_c$ . Bicellar structures have shorter z dimensions and longer x and y dimensions compared to oblate structures.

	Conc. (%)	x-axis ( $r_c$ )	y-axis ( $r_c$ )	z-axis ( $r_c$ )
<b>Tether length = 3</b> <b>Z<sub>channel</sub> = 8<math>r_c</math></b>	10	16±1	13±1	2.0±0.1
	15	16±1	14±1	2.0±0.1
	20	16±1	14±1	2.0±0.1
<b>Tether length = 5</b> <b>Z<sub>channel</sub> = 8<math>r_c</math></b>	10	15±1	13±1	2.1±0.2
	15	15±1	13±1	2.1±0.2
	20	15±1	13±1	2.1±0.1
<b>Tether length = 6</b> <b>Z<sub>channel</sub> = 8<math>r_c</math></b>	10	15±1	13±1	2.1±0.1
	15	15±1	13±1	2.1±0.2
	20	15±1	13±1	2.1±0.2
<b>Tether length = 3</b> <b>Z<sub>channel</sub> = 10<math>r_c</math></b>	10	10±1	8.1±0.4	4.2±0.1
	15	11±2	7±1	4.2±0.1
	20	10±1	8.2±0.4	4.2±0.1
<b>Tether length = 5</b> <b>Z<sub>channel</sub> = 10<math>r_c</math></b>	10	10±1	8.0±0.4	4.2±0.1
	15	10±1	8.0±0.5	4.2±0.1
	20	11±1	7.8±0.6	4.2±0.1
<b>Tether length = 6</b> <b>Z<sub>channel</sub> = 10<math>r_c</math></b>	10	10±1	7.9±0.5	4.2±0.1
	15	10±1	8.1±0.4	4.2±0.1
<b>Tether length = 3</b> <b>Z<sub>channel</sub> = 15<math>r_c</math></b>	10	15±1	5.4±0.3	4.5±0.2
	15	15±1	5.4±0.3	4.5±0.2
	20	15±1	5.4±0.3	4.6±0.2
<b>Tether length = 5</b> <b>Z<sub>channel</sub> = 15<math>r_c</math></b>	10	15±1	5.4±0.3	4.5±0.2
	15	16±1	5.3±0.3	4.4±0.2
	20	15±1	5.4±0.3	4.6±0.2
<b>Tether length = 6</b> <b>Z<sub>channel</sub> = 15<math>r_c</math></b>	10	16±1	5.3±0.4	4.3±0.1
	15	16±1	5.3±0.3	4.4±0.2
	20	15±1	5.4±0.3	4.5±0.1
<b>Tether length = 3</b> <b>Z<sub>channel</sub> = 20<math>r_c</math></b>	10	16±1	5.4±0.4	4.4±0.2
	15	16±1	5.4±0.4	4.4±0.2
	20	15±1	5.4±0.3	4.6±0.2
<b>Tether length = 5</b> <b>Z<sub>channel</sub> = 20<math>r_c</math></b>	10	16±2	5.3±0.4	4.4±0.2
	15	16±2	5.4±0.4	4.4±0.2
	20	16±1	5.4±0.4	4.4±0.2
<b>Tether length = 6</b> <b>Z<sub>channel</sub> = 20<math>r_c</math></b>	10	16±1	5.4±0.4	4.4±0.2
	15	14±1	5.6±0.2	4.7±0.1
	20	14±1	5.5±0.3	4.7±0.2

Table 3.9: The  $x$ ,  $y$ ,  $z$  - principal axes of the self-assembled hairy vesicles for different relative concentrations of the hairy lipids and tether lengths in the confinement with a channel height of  $8r_c$ ,  $10r_c$ ,  $15r_c$  and  $20r_c$ .

We perform interfacial line tension measurements for a hairy vesicle under confinement. We do not observe any influence of confinement over the measurements. However, we find a decrease in line tension with increase in relative concentrations of hairy lipids as shown in Figure 3.11.

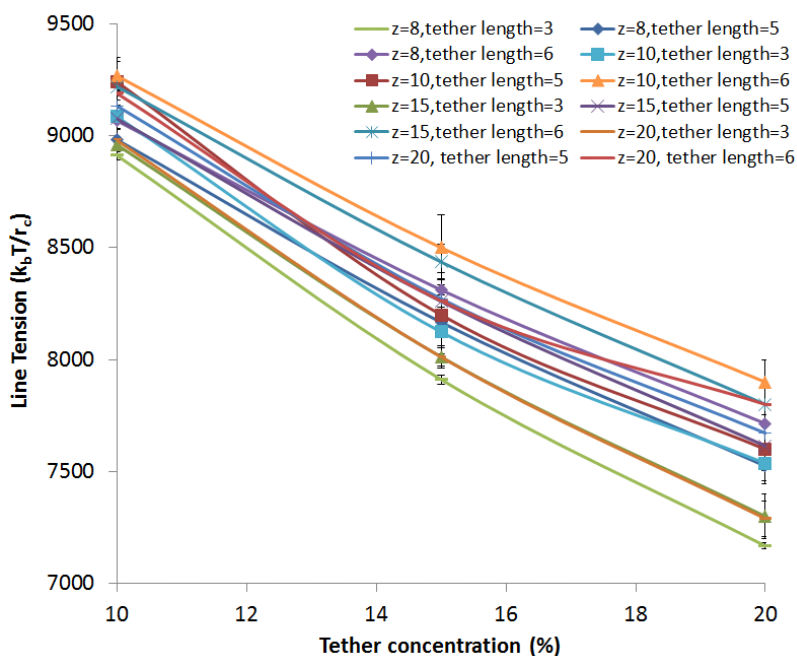


Figure 3.11: A plot of interfacial line tension of the self-assembled hairy vesicles as a function of tether concentration for different distances between two planar surfaces and different tether lengths.

### 3.4 Chapter Conclusions

In this chapter, we have demonstrated the design of a stable hairy vesicle composed of phospholipid and end-functionalized lipid molecules via self-assembly, and identified factors affecting the aggregation dynamics and shape of the equilibrated

aggregate. We broadly classified the factors as intrinsic and extrinsic factors. The intrinsic factors we discussed include relative concentration of hairy lipids, tether length, molecular stiffness, degree of distinction between hydrocarbon tails. We focused on volumetric confinement being our only extrinsic factor. We calculated the scaling exponents with respect to number of clusters and average cluster size to characterize the dynamics of cluster growth at latter times of self-assembly. We have demonstrated that higher tether length and relative concentration of hairy lipids decelerates the cluster growth in bulk conditions. In confined conditions, it was found that higher degree of confinement promotes cluster growth and under such circumstances less effect is observed due to intrinsic factors like tether length and relative concentration of hairy lipids. We demonstrate that the disproportionate distribution of the hairy lipid molecules across the monolayers is due to the excluded volume of the tethers, which is in good agreement with theoretical and experimental results<sup>31,33</sup>. We concluded that shape of vesicle in bulk conditions depends upon the interplay between packing of species and excluded volume of tethers. A good agreement with experimental studies<sup>34,113-114</sup> was achieved in this regard. We demonstrated the transition of shape from prolate to oblate to bicellar structure with increase in degree of confinement. These observations are in good agreement with theoretical investigations that demonstrate formation of oblate vesicles from prolate vesicles at high degree of confinement<sup>111</sup>.

## Chapter 4 Interactions of Bald and Hairy Vesicles with Nanoparticles

The publications relevant to details of the discussions provided in this section:

- Aydin, F., **Uppaladadium, G.**, Dutt, M., Harnessing Steric Hindrance to Control Interfacial Adsorption of Patchy Nanoparticles onto Hairy Vesicles 141, 458-466.
- **Uppaladadium, G.**, Aydin, F., Dutt, M., Modeling interactions between charged nanoparticles and multi-component vesicles. In preparation.

### Contributions to this work:

- Running the simulations
- Performing the analysis and visualization of the system
- Writing a manuscript under preparation

### 4.1 General Overview

The interaction of nanoparticles (NPs) with specific binding sites with macromolecules is a topic of interest as these nanoparticles through adsorption, are capable of affecting the morphology of liposomes which are promising drug delivery vehicles<sup>115</sup>. The surfaces of liposomes employed for therapeutic purposes are designed in a way so as to reduce adsorption of certain proteins called opsonins, which make the liposome more vulnerable to phagocytosis by macrophages.<sup>116-120</sup> Inspired from the cell membranes, certain polymer chains can be grafted on to liposome surface to mitigate protein adsorption on to the surface.<sup>115</sup> Grafting of polymer chains onto the surface also serves to increase the circulation time and steric stability<sup>29-33</sup> of the vehicle. PEG is a widely used polymer chain for this purpose and experimental studies in the past have

been conducted in order to understand the interactions between PEGylated vesicles and plasma proteins like fibrinogen, hemoglobin and cytochrome c.<sup>121-123</sup> An attempt has been made to understand the factors affecting and the mechanisms of interaction between functionalized NPs and vesicles through a computational study. An MD-based mesoscopic simulation technique entitled Dissipative Particle Dynamics (DPD)<sup>2,41,57,88,91</sup> has been used for this purpose. In this chapter we investigate interactions of functionalized NPs with bald and hairy vesicles respectively. We investigate how adsorption of these NPs affects the morphology of a bald vesicle and the role of length and grafting density of tethers emanating from the vesicle and size of the NPs affect the adsorption process.

## 4.2 Adsorption of functionalized NPs onto bald vesicle surface

### 4.2.1 Modeling and system setup

System consists of a three lipid species and patchy NP's as shown in Figure 4.1.

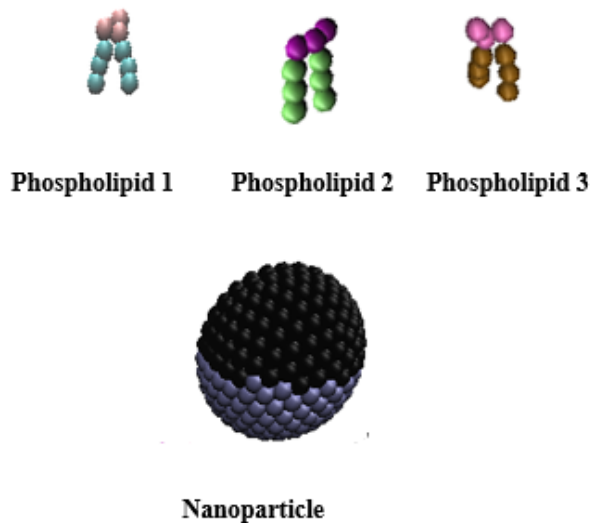


*Figure 4.1: Coarse-grained structure of individual species present in the bald vesicle-NP system*

The liposomes are composed of three different species of phospholipids in 1:1:1 ratio. We begin with a pre-assembled liposome, which is equilibrated in a simulation of box with  $40r_c \times 40r_c \times 40r_c$  as its dimensions over a time interval of  $30,000 \tau$ . The simulation box has a bead density of 3, as a result of which the box contains 192,000 beads. The simulation box has periodic boundaries along the co-ordinate axes and houses a total of 1178 phospholipid molecules. Eight NPs are introduced into the simulation box beyond the interaction range of the liposome surface. The bead capacity of the simulation box is always conserved by replacing the corresponding amount of solvent beads with NP beads when a NP is introduced. The NPs are hollow spheres composed of 312 hydrophilic beads with different patch sizes. The distance between the centers of neighboring beads of the NP is set to  $0.5 r_c$ . We investigate the interaction between NPs and liposomes for the following patch sizes of NPs: (i) 10% of the NP surface, (ii) 30% of the NP surface, (iii) 50% of the NP surface.

The soft repulsive interaction parameters between different moieties of the system are given in Table 4.1.

$a_{ij}(k_B T/r_c)$	Head 1	Tail 1	Head 2	Tail 2	Head 3	Tail 3	NP	Patch	Solvent
<b>Head 1</b>	25	100	50	100	50	100	25	25	25
<b>Tail 1</b>	100	25	100	25	100	25	100	100	100
<b>Head 2</b>	50	100	25	100	50	100	25	5	25

<b>Tail 2</b>	100	25	100	25	100	25	100	100	100
<b>Head 3</b>	50	100	50	100	25	100	25	25	25
<b>Tail 3</b>	100	25	100	25	100	25	100	100	100
<b>NP</b>	25	100	25	100	25	100	50	50	25
<b>Patch</b>	25	100	5	100	25	100	50	50	25
<b>Solvent</b>	25	100	25	100	25	100	25	25	25

*Table 4.1: Soft repulsive interaction parameters,  $a_{ij}$  between moieties of the system where 'i' represents the species in the columns and 'j' represents the species in the rows.*

Favorable enthalpic interactions take place between patch and one of the phospholipid head groups. The repulsion between the NPs can represent the electrostatic repulsion between identically charged NPs.

## 4.2.2 Results and Discussions

### 4.2.2.1 Mechanism of Adsorption

8 NPs with patch covering 10% of the surface are placed at random positions in the simulation box containing an equilibrated liposome. The initial system configuration is shown in Figure 4.2. We find from our results that, the adsorption depends on: (1) orientation of NPs with respect to the liposome, (2) availability of preferred phospholipid head groups on surface of the liposome, (3) whether the NP patch and the phospholipid head groups to which the patch is attracted to, are in interaction range. The NPs are found to diffuse in the solvent until a patch comes into the interaction range of the preferable phospholipid head group. A pair of beads is considered to be in interacting range if the center-to-center distance is less than the interaction cut-off distance ( $r_c=1$ ). The highly

favorable enthalpic interactions between NP patch and preferable head group leads to adsorption onto the liposome surface.

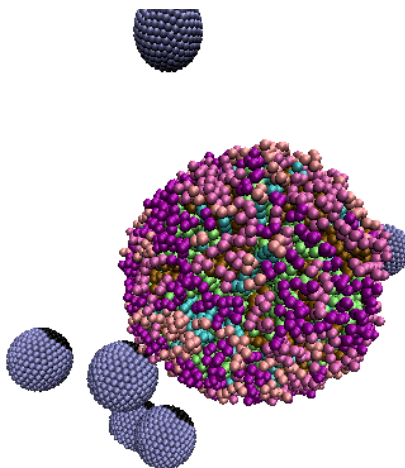


*Figure 4.2: Initial configuration of the bald vesicle-NP system*

We examine the time evolution of the number of interactions for different patch sizes of NPs and multiple seeds. The continuous increase in the number of NP patch and head beads interactions after initial contact of NP patch with phospholipid head group suggests that the adsorption on to the liposome surface is permanent. Following the initial interaction, there is a steep increase in the number of interactions between the patch and the phospholipid head groups. The number of interactions subsequently reaches a steady-state indicating the completion of adsorption of all NPs. From Figure 4.3, it can be observed that all runs do not reach the steady-state at the same time. We repeat the experiment with patch size of 30% and 50%.

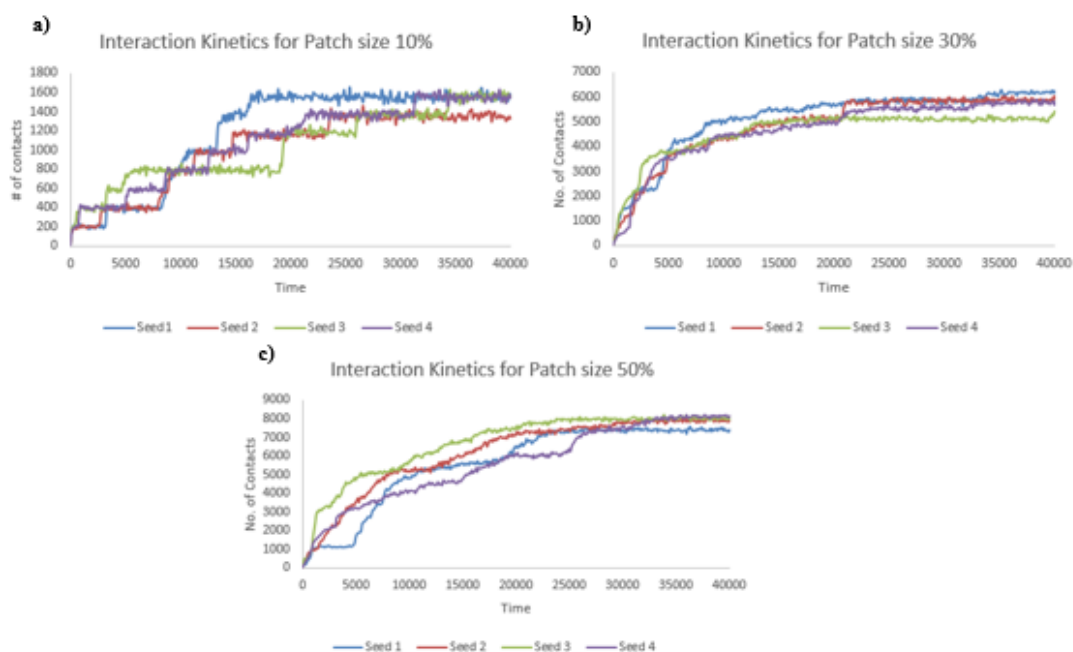
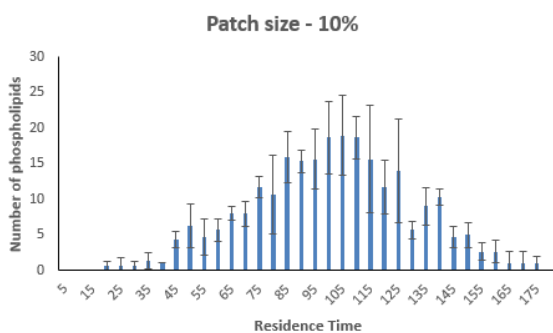


Figure 4.3: Increase of number of contacts with time until  $40000 \tau$  between liposome and NPs with patch size **a)** 10%, **b)** 30%, **c)** 50%.

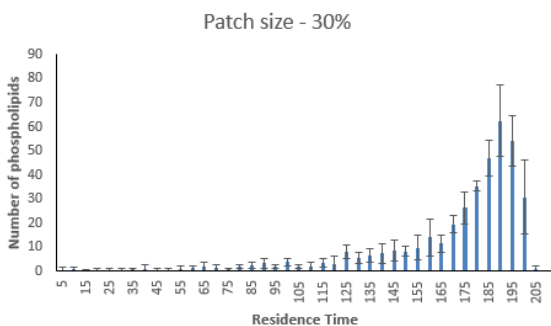
We measure the residence time to understand the dynamics of the phospholipids interacting with the NPs following their adsorption. We define the residence time as the number of times a phospholipid molecule is found to be interacting with a NP patch during a time interval spanning  $10,000\tau$ . For this measurement, we measure the interactions between the phospholipid head groups and the NP patch at time intervals of  $50\tau$ . The residence time distribution is obtained by binning the number of phospholipid molecules based with a given residence time. For these measurements we use NPs with 10%, 30%, 50% patch size as respectively shown in Figure 4.4. The phospholipid molecules diffuse in the bilayer until they are within interaction range of the NP patch. These molecules will interact with the patch for a short time interval before diffusing

away. This behavior is captured by a large population of phospholipid molecules with short residence times. We observe an increase in the residence time of the phospholipids with the number of NPs, as shown by the residence time distribution shifting towards the right. We infer that a large patch results in a smaller number of phospholipids that are free to diffuse in the bilayer, and can contribute to the population of phospholipids interacting with the patch but are in flux. The simulations have been run for a total time of  $10,000\tau$  and each data point has been averaged over four simulation runs using different random seeds.

a)



b)



c)

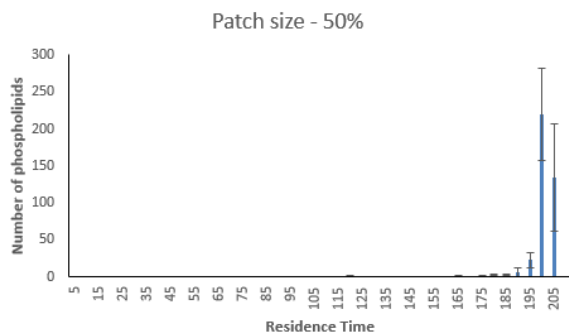


Figure 4.4: Residence time measurements of NPs with patch sizes of (a) 10%, (b) 30%, (c) 50% following their adsorption on to the phospholipid head groups.

#### 4.2.2.2 Effect of Adsorption on morphology of bald vesicle

We have also examined the deformations induced by the NPs over the liposomes during the adsorption process. In order to do this, we assume the final shape of the liposome post-adsorption to be an ellipsoid. We then measure the highest distance along which the ellipsoid is spread along x, y, z axes. We run simulations for 10%, 30%, 50% patch sizes, and the results obtained are averaged over 4 random seeds and tabulated in Table 4.2.

	Patch size 10%			Patch size 30%			Patch size 50%		
	Xmax	Ymax	Zmax	Xmax	Ymax	Zmax	Xmax	Ymax	Zmax
<i>Ellipsoi</i>	8.9±0.	8.4±0.	7.3±0.	10.8±1.	7.8±0.	6.6±0.	11.2±1.	9.8±1.	6.2±1.
<i>d radii</i>	2	1	1	0	3	6	3	2	1

Table 4.2: A comparison of the dimensions of the liposomes for different patch sizes of NPs at end of simulation.

From the above results a transformation of shape from a spherical form to a more ellipsoidal form can be observed with increase in the patch size of the NPs. Wang et al., observed that adsorption of NPs leads to surface reconstruction of liposomes by changing the orientation of lipid head groups with respect to the tails.<sup>124</sup> The pictorial representation of their observations is as shown in Fig 4.5.

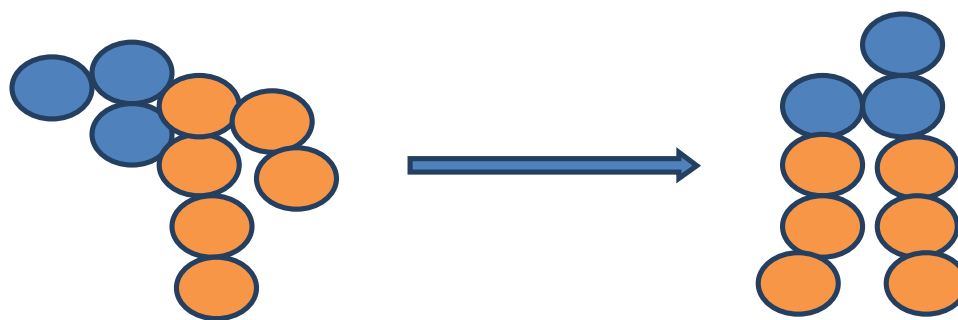


*Figure 4.5: Binding of nanoparticles to the liposome surface causes reorientation of the lipid head groups reducing the area per lipid of the molecule.*

We observe formation of hydrophilic domains at the site of NP adsorption. This is observed because the reorientation of lipid head groups at the site of adsorption causes decrease in area per lipid of the lipid molecules present there. This indicates that NP templates a gel phase at the site of adsorption. This difference of area per lipid of molecules at the site of adsorption and rest of the liposome surface causes deformation of the liposome.

### 4.3 Effect of grafted tethers on Adsorption

#### 4.3.1 System description

The system consists of a stable hairy vesicle composed of phospholipid and hairy lipid molecules<sup>94</sup>, and patchy NPs in a hydrophilic solvent. Individual phospholipid molecules are represented by bead spring models, and consist a hydrophilic head group with three beads and two hydrophobic hydrocarbon tails consisting of three beads each. The tethers grafted to the head group of one of the phospholipid molecules are modeled by three and six hydrophilic beads, corresponding to short and long tethers respectively. Oligo ethylene glycol (OEG) chains with a degree of polymerization of 6 and 12 serve as good experimental examples. In fact, previously experimental studies<sup>125</sup> have been carried out using OEG grafted lipid systems with OEG chains having average molecular of 350 and 750 g/mol.

The nanoparticles employed in this system are hydrophilic hollow spheres composed of 312 beads with patch covering 20% of the surface as shown in Figure 4.6. Experimental examples can be proteins, drug molecules or metallic NPs with functional chains grafted to their surface<sup>121</sup>. The complex topography and asymmetric charge distribution is modeled into a patchy spherical NP<sup>126</sup>. Different sizes of NPs are used which respectively correspond to 50%, 100%,150% of the length of long tethers. They have the following radii:  $0.75r_c$  (small NP),  $1.50r_c$  (medium NP),  $2.25r_c$  (large NP).

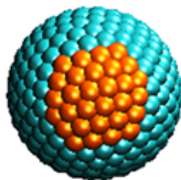


Figure 4.6: Spherical patchy NP with a radius of  $2.25r_c$

The hairy vesicles are composed of phospholipids and hairy lipids<sup>94</sup> in a 1:1 ratio. We begin with a pre-assembled liposome which is equilibrated in a simulation of box with  $40r_c \times 40r_c \times 40r_c$  as its dimensions over a time interval of  $10,000 \tau$ . The simulation box has a bead density of 3, as a result of which the box contains 192,000 beads. The simulation box has periodic boundaries along the co-ordinate axes and houses a total of 1178 phospholipid molecules. We examine hairy lipids with short and long tethers. The hairy vesicle measures nearly  $7r_c$  in radius excluding the tethers. NPs are introduced into the simulation box beyond the interaction range of the liposome surface. The bead capacity of the simulation box is always conserved by replacing the corresponding amount of solvent beads with NP beads when a NP is introduced. The simulations are run until all the NPs are interfacially adsorbed on to the vesicle. The characterization for each system uses particle trajectories from four simulations which have identical initial conditions but different random seeds. We examine two different scenarios, classified based on the moiety NP patch has favorable interactions with. First scenario being, where NP patch has favorable enthalpic interactions with phospholipid head groups.<sup>123</sup> In this scenario we investigate for both tether lengths. The second scenario being, where NP patch has favorable enthalpic interactions with tethers. In this part, we focus on longer tether length which is of more experimental relevance.<sup>28,31,32</sup>

#### **4.3.2 NP patch- Phospholipid head group interaction driven adsorption**

Initially, a hairy vesicle along with 4 large NPs placed outside the interaction range of the vesicle at random locations, is placed in the simulation box. The initial configuration of the system, for both short and long tethers grafted on to the phospholipid

head group of the vesicle is as shown in Figure 4.7 (a) and 4.7 (b). Factors affecting the adsorption process are:

- (i) Deterrence offered by tethers to the approaching NPs.
- (ii) Orientation of the NPs in a way that the patch faces the phospholipid head group.
- (iii) Presence of NP patch within the interaction range of the phospholipid head group.

The contact of NP patch with phospholipid head group due to its highly favorable enthalpic interaction is termed as adsorption. From our results, it is observed that NPs diffuse in solvent until they bypass the tethers and fall within the interaction range of the phospholipid head group. This holds good for hairy vesicle irrespective of the tether length as shown in Figure 4.7 (c) and 4.7 (d).

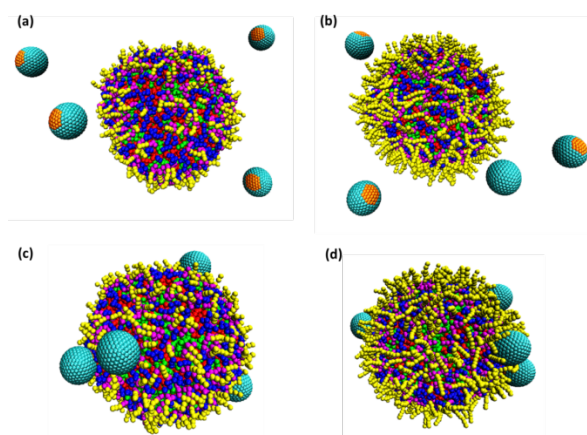


*Figure 4.7: Initial configuration of (a) binary component hairy vesicle composed of phospholipids (50%) and hairy lipid molecules with short tethers (50%), and 4 NPs placed outside the interaction range of the hairy vesicle, (b) binary component hairy*

*vesicle composed of phospholipids (50%) and hairy lipid molecules with long tethers (50%), and 4 NPs placed outside the interaction range of the hairy vesicle, (c) short tether hairy vesicle with 4 NPs adsorbed onto the phospholipid head groups at  $t = 160,000\tau$ , (d) long tether hairy vesicle with 4 NPs adsorbed onto the phospholipid head groups at  $t = 160,000\tau$ .*

When the number of interactions between the NPs and long tethers were captured as a function of time, it was observed that NPs are constantly hitting the hairy vesicle surface and are quite often pushed away by the tethers as they are diffusing in the solvent. The number of interactions between NPs and tethers as a function of time is shown in Figure 4.8.

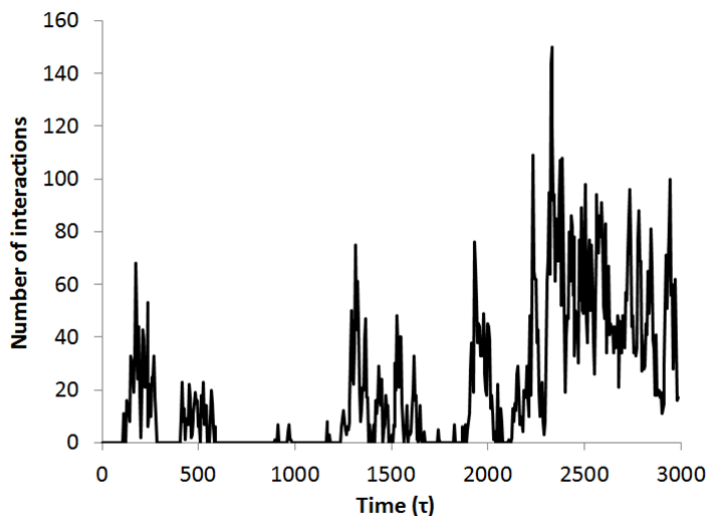


*Figure 4.8: A plot of number of interactions between nanoparticle and tethers as a function of time for 4 nanoparticles interacting with hairy vesicle composed of long tethers.*

High tether density promotes steric stabilization and hinders interfacial adsorption due to high conformational entropy.<sup>2</sup> Hence, the NPs and phospholipid head groups reach close proximity in areas with low tether density. Some NPs are observed to bypass the tethers as shown in Figure 4.9 (a) and 4.9 (b). Once the NPs have a close proximity with the phospholipid head group, the NPs are observed to re-orient themselves such that the patch faces and comes within the interaction range of the nearest phospholipid head group as shown in Figure 4.9 (c). Subsequently, the first interaction occurs as shown in Figure 4.9 (d). The first interaction activates the subsequent adsorption of NPs onto the vesicle surface as shown in Figure 4.9 (e) and 4.9 (f). This is justified by the steep increase in the number of interactions post first interaction until the number of interactions reach a steady value as shown in Figure 4.9 (g). Each NP patch is found to be interacting with 6-8 phospholipid molecules. The NPs are found to be mobile on the vesicle surface with constant change in the phospholipid molecules interacting with the patch. However, the number of phospholipid molecules interacting is found to remain nearly constant once the number of interactions, reach a steady value.

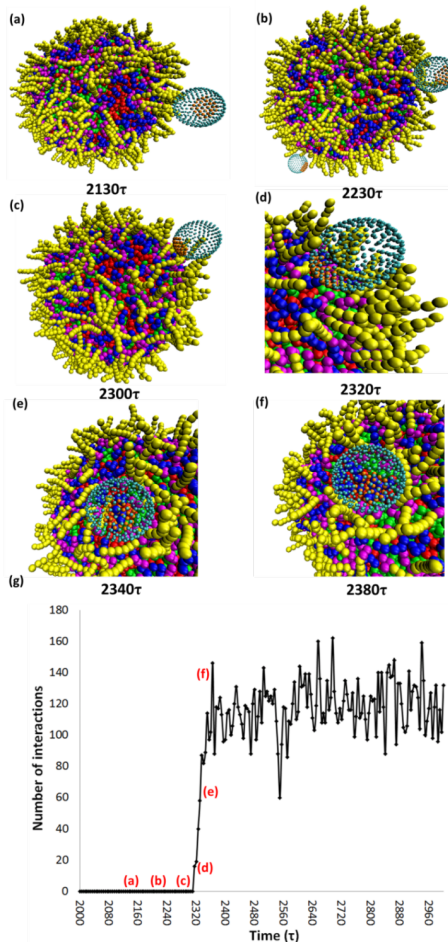


*Figure 4.9: Images of the capture of a single NP by phospholipid head groups of a hairy vesicle composed of long tethers at (a)  $t = 2130\tau$ , (b)  $t = 2230\tau$ , (c)  $t = 2300\tau$ , (d)  $t = 2320\tau$ , (e)  $t = 2340\tau$ , (f)  $t = 2380\tau$  and (g) a plot of the number of interactions between NP patch and tethers as a function of time during the capturing process.*

We expect long intervals of time between the adsorption of two individual NPs. This is because of higher steric hindrance exerted by the tethers on approaching NPs due to their larger excluded volume. It is observed that adsorption is quicker onto vesicles with shorter tethers compared to those of longer tethers as shown in Figure 4.10.

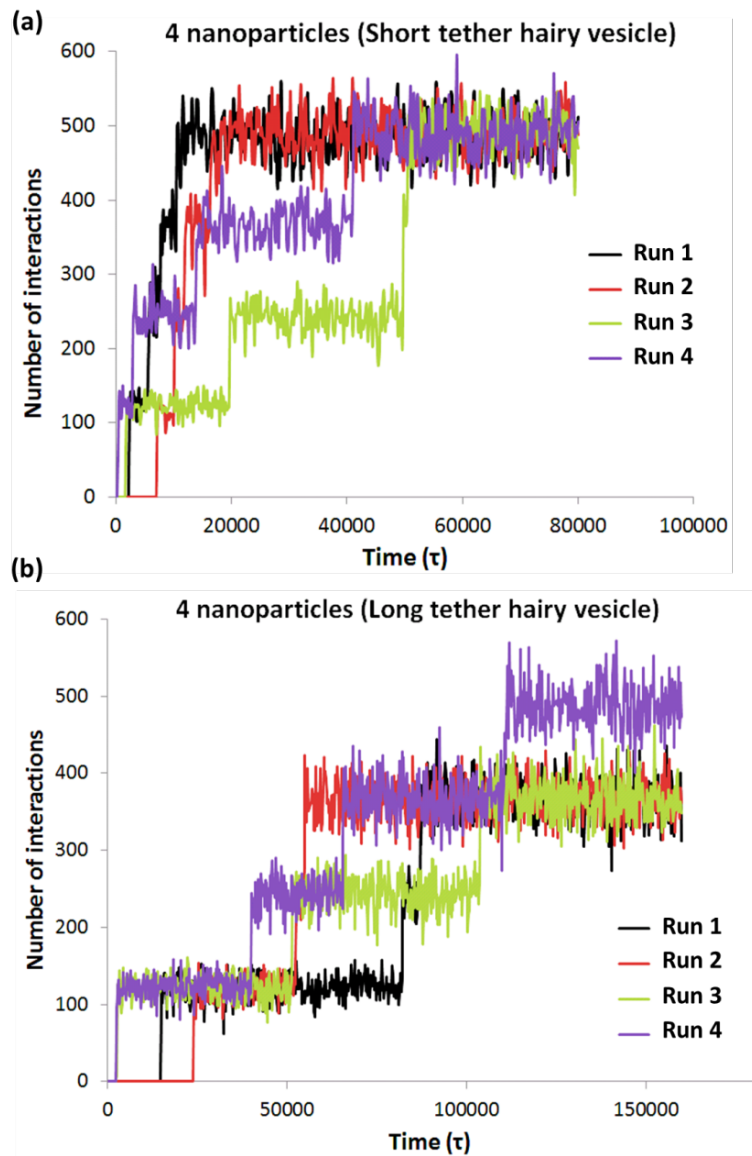


Figure 4.10: Plots of the number of interactions between the NP patch and phospholipid head groups as a function of time for 4 NPs interacting with hairy vesicle composed of (a) short and (b) long tethers. The simulations of hairy vesicles composed of short and long tethers have been run for a total time of  $80,000\tau$  and  $160,000\tau$ , respectively. The measurements from four simulation runs using different random seeds are shown separately in the plot.

The same study is repeated with 8 and 12 NPs. It is observed that the increase in NPs leads to decrease in adsorption time per NP as shown in Figure 4.11.

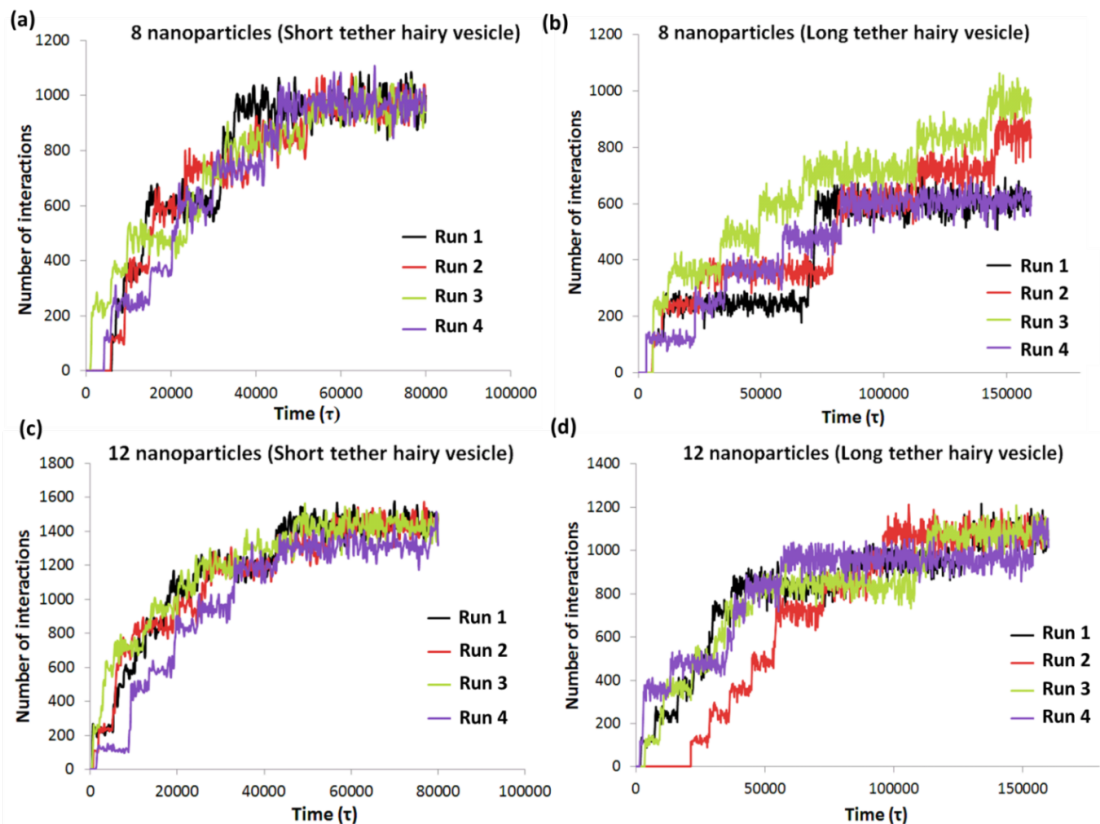


Figure 4.11: Plots of number of interactions between nanoparticle patch and phospholipid head groups as a function of time for (a) 8, (b) 12 nanoparticles interacting with hairy vesicle composed of short tethers and (c) 8, (d) 12 nanoparticles interacting with hairy vesicle composed of long tethers. The simulations of hairy vesicles composed of short and long tethers have been run for a total time of  $80,000\tau$  and  $160,000\tau$ , respectively. The measurements of four simulation runs using different random seeds are shown separately in the plot.

Unfavorable enthalpic interactions between the NPs, pushing the NPs towards the vesicle surface could be a convincing explanation for the above phenomena, since this would accelerate the adsorption of NPs onto the vesicle surface.

To study the role of tether concentration on the adsorption time of NPs, we measure the number of NPs adsorbed in a time interval of  $30,000\tau$  for a range of relative concentration of the hairy lipids spanning 10% to 50%. 12 NPs and vesicles with short and long tethers are used for this purpose. We observe that small NPs do not get adsorbed on to the vesicle surface with long tethers irrespective of the tether concentration. For NPs with larger sizes, the number of adsorbed NPs decrease linearly with increase in the relative concentration of long tethers, as shown in Figure 4.12. Similar trends are found for the small and medium sized NPs adsorbing on to vesicles grafted with short tethers.

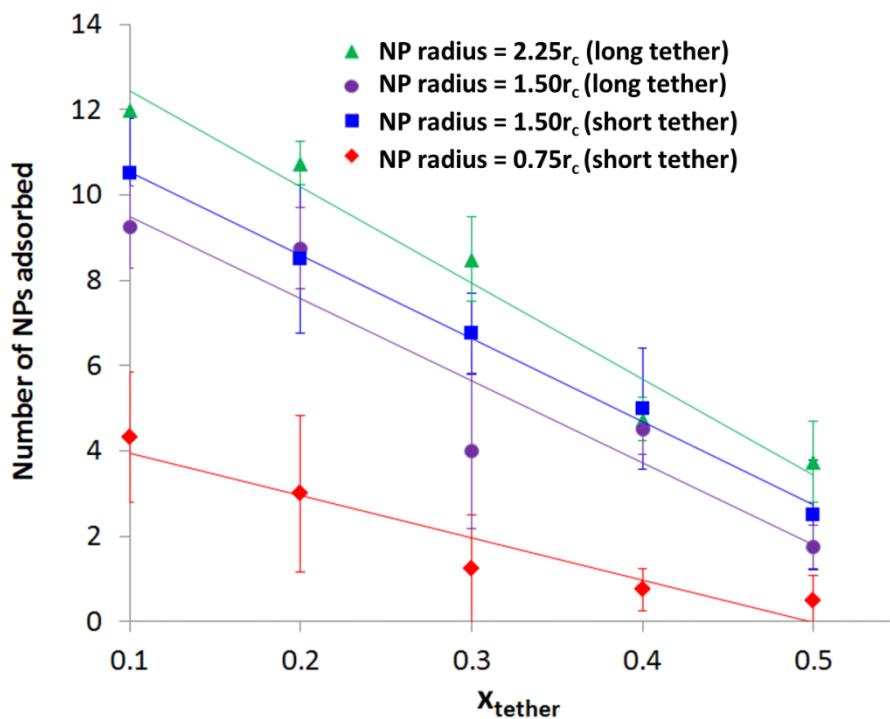


Figure 4.12: A plot of the number of NPs adsorbed on to the phospholipid head groups of hairy vesicle composed of short and long tethers as a function of tether composition (0.1

to 0.5) respectively for the NP radius of  $0.75r_c$  and  $1.50r_c$ , and the NP radius of  $1.50r_c$  and  $2.25r_c$ . The simulations have been run for a total time of  $30,000\tau$  and each data point has been averaged over four simulation runs using different random seeds.

These observations are in good agreement with previous theoretical<sup>97</sup> and experimental results<sup>98,99</sup>, that report a linear decrease in the adsorption of proteins on a gold surface grafted with oligomeric polyethylene oxide chains owing to their high entropic repulsions. The difference in the number of adsorbed NPs is small when the size of the NPs is comparable to the length of the tethers. There is no adsorption when the size of the NPs is smaller than the tether length. These observations agree with studies that show that amount of protein adsorbed on the surface becomes independent of the polymer chain length when the thickness of the polymer layer is greater than the protein size.<sup>127</sup>

We conduct residence time measurements for this system. For these measurements we use 4, 8 and 12 large NPs and hairy vesicles with short and long tethers as shown in Figure 4.13. The molecules are found to interact with patch for a short interval of time before diffusing away. This behavior is captured by a large number of phospholipid molecules having short residence times. The residence time distribution is observed to shift to the right with increase in the number of NPs because of smaller number of phospholipids that are free to diffuse in the vesicle. The simulations have been run for a total time of  $10,000\tau$  and each data point has been averaged over four simulation runs using different random seeds.

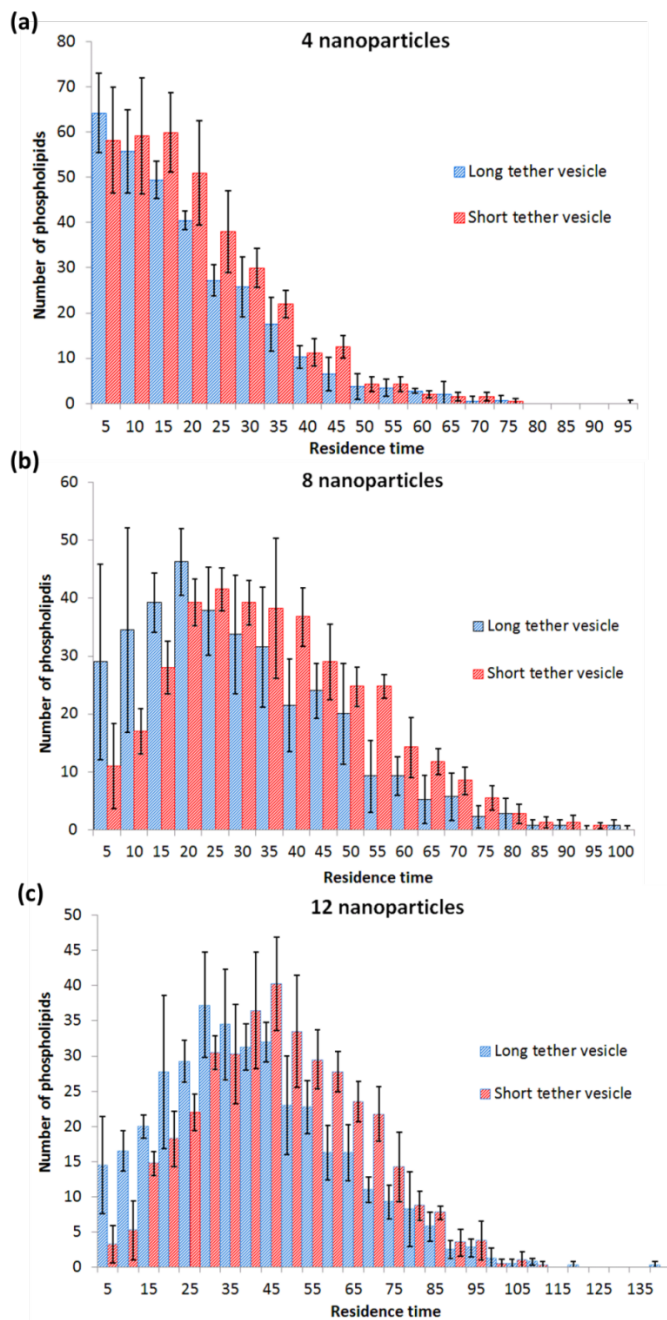


Figure 4.13: Residence time measurements of NPs after their adsorption on to the phospholipid head groups of hairy vesicle composed of short and long tethers for (a) 4, (b) 8 and (c) 12 NPs.

### 4.3.3 NP patch- Tether interaction driven adsorption

These studies have been carried on a hairy vesicle - NP system with long and short tethers. 4, 8 and 12 NPs have been used. In this case, all interaction parameters are as in Table 4.1 except for that interaction parameter between patch and head2 is set at  $a_{ph2} = 25$  and that between patch and tether is set at  $a_{pT} = 5$ .

The observations made are similar to those made in the case of adsorption driven by NP patch- phospholipid head group interaction. The NPs are found to diffuse in the solvent until they fall within the interaction range of the tethers. The adsorption of NP on to the tethers is activated by the first interaction with a tether. Post interactions, the NP reorients itself such that the number of interactions with the tethers increases and reaches a steady value. All these observations are shown in Figure 4.14. The NPs are observed to diffuse over the vesicle surface post adsorption onto the tethers.

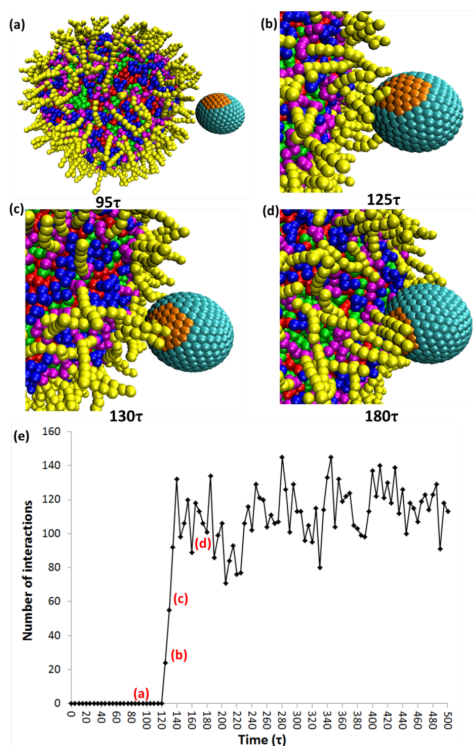
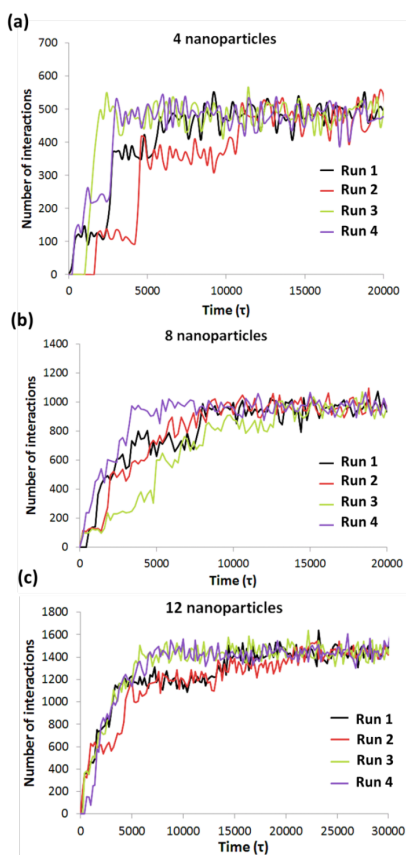


Figure 4.14: Images of the capture of single NP by tethers of hairy vesicle composed of long tethers at (a)  $t = 95\tau$ , (b)  $t = 125\tau$ , (c)  $t = 130\tau$ , (d)  $t = 180\tau$ , and (e) a plot of number of interactions between NP patch and tethers as a function of time during the capturing process.

The time evolution of the interaction count between the patch and tethers, for different number of NPs is as shown in Figure 4.15. The contrast between the head-patch and patch-tether interaction plots is that the discrete increase is the interaction count is missing in the latter. Due to lack of steric hindrance, the time required for adsorption of all NPs onto tethers is shorter than the time required for adsorption of NPs onto the phospholipid head groups.



*Figure 4.15: Plots of number of interactions between NP patch and tethers as a function of time for (a) 4, (b) 8, (c) 12 NPs interacting with hairy vesicle composed of long tethers. The simulations have been run for a total time of  $80,000\tau$ . The measurements from four simulation runs using different random seeds are shown separately in the plot.*

We conduct residence time studies for this system with patch-tether interactions over a time interval of  $10,000\tau$  for 4, 8, 12 large NPs introduced into the solvent at random locations simultaneously. Interactions are tracked at intervals of  $50\tau$ . To understand the difference in behavior of the NPs adsorbed onto phospholipid head groups and tethers, we compare the residence time distributions of both the systems. The comparative residence time measurements for systems with favorable interactions of patch with phospholipid head group with short tethers and patch with long tethers are shown in Figure 4.16. We observe that the interactions between patch and tethers are primarily short termed. We believe that the conformational entropy of the tethers impacts the duration of interaction. Also, the NPs adsorbed onto the head groups experience high obstruction from the tethers with high excluded volume hindering their lateral diffusion on the vesicle surface, which as a result increases the duration of their interaction with the head groups. Previous experiments have already demonstrated a decrease in lateral diffusion of adsorbed proteins on a liposome surface grafted with PEG chains due to the obstruction caused by tethers.<sup>123</sup>

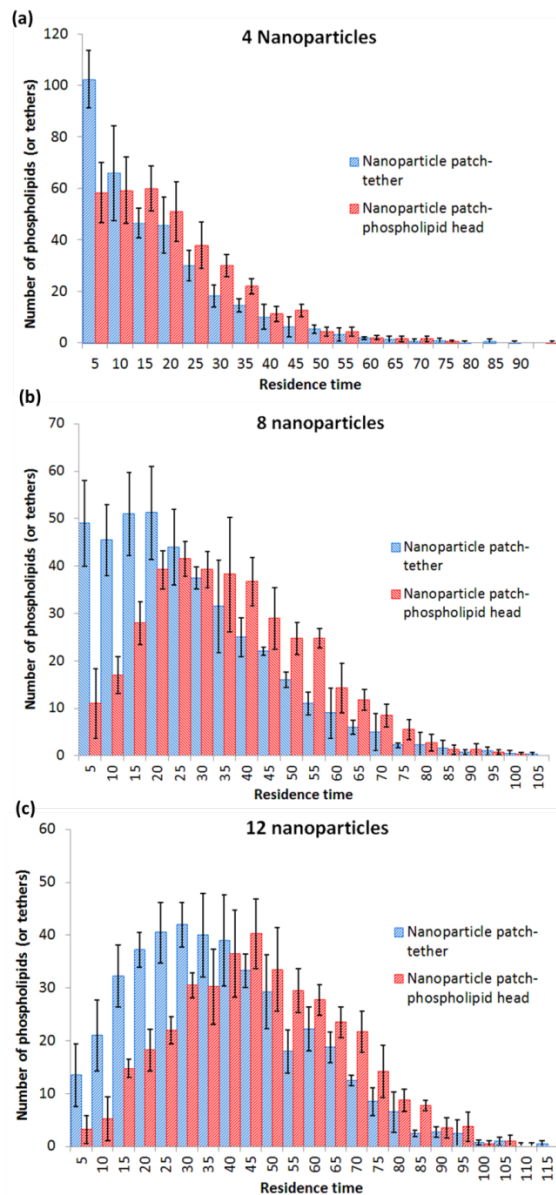


Figure 4.16: Residence time measurements of NPs following their adsorption on to the phospholipid head groups of the hairy vesicle composed of short tethers and tethers of hairy vesicles composed of long tethers for (a) 4, (b) 8 and (c) 12 NPs. The simulations have been run for a total time of  $10,000\tau$  and each data point has been averaged over four simulation runs using different random seeds.

#### 4.4 Chapter Conclusions

In this chapter, we have studied the interfacial adsorption of NPs over bald macromolecules and sterically stabilized vesicles. We have demonstrated that adsorption of NPs onto vesicle surface without grafted tethers is permanent. Our results also demonstrate that the vesicle morphology varies from spherical to ellipsoidal with increase in the patch size. Our observations are in good agreement with experimental studies<sup>124</sup> which demonstrate surface reconstruction occurring due to reorientation of phospholipid molecules.

We have identified that NP size relative to tether length, relative concentration of hairy lipids, relative affinity of patch towards tethers and phospholipid head group influence the adsorption characteristics of the NPs. The NPs are found to adsorb less on the surface of vesicle with higher relative tether concentration. This observation is in good agreement with previous theoretical and experimental studies.<sup>97-99</sup> Our residence time measurements indicate the NPs to be laterally diffusing over the vesicle surface and being obstructed by presence of tethers. This is in a good agreement with experimental results.<sup>123</sup>

## Chapter 5 Conclusions

Investigations on bio-inspired macromolecules were carried out querying the role of intrinsic and extrinsic factors on the organization, stiffness, shape and stability of the vesicles. Investigations were also carried out to understand the interactions of vesicles with functionalized nanoparticles. For this purpose, we used DPD to capture the hydrodynamic effects of the system. DPD enabled us to resolve the dynamics over a large length and time scales.

In chapter 3, we developed coarse-grained models for vesicle constituents. We investigated the self-assembly dynamics of the amphiphilic species and concluded that greater tether lengths and greater relative concentration of hairy lipids in the system decelerates the cluster growth. We studied the effect of intrinsic properties like tail stiffness, tether length and relative tether concentration, dissimilarity between species on the morphology of the vesicle. We demonstrated that increased dissimilarity between the phospholipid tail groups leads to domain formation and macroscopic phase segregation over the surface. We found our results to be in good agreement with various theoretical and experimental results. We also studied the effect of extrinsic factors like volumetric confinement on the morphology of interfacially stable hairy vesicles. We demonstrated the shape transition from prolate to oblate to bicellar structures with increasing degree of confinement. We found these observations to be in good agreement with previous theoretical investigations.

In chapter 4, we demonstrated that adsorption of NPs onto bald vesicles is permanent. We also concluded that higher patch sizes induces reorganization of vesicle

constituents causing morphological changes from spherical to ellipsoidal morphology. This is in good agreement with previous experimental results. We also demonstrated that relative concentration of hairy lipids, NP size relative to tether length to affect the adsorption of NPs onto phospholipid heads groups and tethers on a hairy vesicle respectively. We found the amount of NPs absorbed to reduce with decrease in NP size with respect to tether length. The same is observed when the relative concentration of hairy lipids increases, which is in good agreement with experimental and theoretical studies. We observed that NPs laterally diffuse over the surface post adsorption and their lateral diffusion is obstructed by tethers.

On a final note, this thesis is focused on understanding the affect of intrinsic and extrinsic properties on structural, morphological characteristics and interfacial stability of biomacromolecules and their interactions with NPs over large length and time scales.

## References

1. Alberts, B.; Johnson, A.; Lewis, J.; Raff, M.; Roberts, K.; Walter, P. *Molecular Biology of the Cell*. Garland Science: New York, 2007.
2. Laradji, M.; Kumar, P.B.S. Dynamics of Domain Growth in Self-assembled Fluid Vesicles. *Phys. Rev. Lett.* **2004**, *93*, 198105.
3. Veatch, S. L.; Keller, S. L. Separation of Liquid Phases in Giant Vesicles of Ternary Mixtures of Phospholipids and Cholesterol. *Biophys. J.* **2003**, *85*, 3074–3083.
4. Lipowsky, R. Budding of Membranes Induced by Intramembrane Domains. *J. Phys. II* **1992**, *2*, 1825.
5. Esposito, C.; Tian, A.; Melamed, S.; Johnson, C.; Tee, S-Y.; Baumgart, T. Flicker Spectroscopy of Thermal Lipid Bilayer Domain Boundary Fluctuations. *Biophys. J.* **2007**, *93*, 3169-3181.
6. Ramachandran, S.; Laradji, M.; Kumar, P.B.S. Lateral Organization of Lipids in Multi-component Liposomes. *J. Phys. Soc. Jpn.* **2009**, *78*, 041006.
7. Stanich, C.A.; Honerkamp-Smith, A.R.; Putzel, G.G.; Warth, C.S.; Lamprecht, A.K.; Mandal, P.; Mann, E.; Hua, T.-A.D.; Keller, S.L. Coarsening Dynamics of Domains in Lipid Membranes. *Biophys. J.* **2013**, *105*, 444-454.
8. Taniguchi, T. Shape Deformation and Phase Separation Dynamics of Two-component Vesicles. *Phys. Rev. Lett.* **1996**, *76*, 4444-4447.
9. Fan, J.; Han, T.; Haataja, M. Hydrodynamic Effects on Spinodal Decomposition Kinetics in Planar Lipid Bilayer Membranes. *J. Chem. Phys.* **2010**, *133*, 235101.
10. Bagatolli, L.A.; Gratton, E. Direct Observation of Lipid Domains in Free Standing Bilayers Using Two-photon Excitation Fluorescence Microscopy. *J. of Fluorescence* **2001**, *11*, 141-160.
11. Ramachandran, S.; Komura, S.; Gommper, G. Effects of an Embedding Bulk Fluid on Phase Separation Dynamics in a Thin Liquid Film. *EPL* **2010**, *89*, 56001.
12. Ursell, T.S.; Klug, W.S.; Phillips, R. Morphology and Interaction between Lipid Domains. *Proc. Natl. Acad. Sci. USA* **2009**, *106*, 13301.
13. Bagatolli, L.; Kumar, P.B.S. Phase Behavior of Multicomponent Membranes: Experimental and Computational Techniques. *Soft Matter* **2009**, *5*, 3234-3248.
14. Cooke, I. R.; Kremer, K.; Deserno, M. Tunable Generic Model for Fluid Bilayer Membranes. *Phys. Rev. E.* **2005**, *72*, 011506.
15. Marrink, S. J.; de Vries, A. H.; Tieleman, D. P. Lipids on the Move: Simulations of Membrane Pores, Domains, Stalks and Curves. *Biochim. Biophys. Acta, Biomembr.* **2009**, *1788*, 149–168.
16. Boal, D. *Mechanics of the cell*. Cambridge University Press: New York, 2012.
17. Liang, X.; Mao, G.; Ng, K.Y.S. Mechanical Properties and Stability Measurement of Cholesterol-containing Liposome on Mica by Atomic Force Microscopy. *J. Colloid Interface Sci.* **2004**, *278*, 53–62.
18. Baumgart, T.; Das, S.; Webb, W.W.; Jenkins, J.T. Membrane Elasticity in Giant Vesicles with Fluid Phase Coexistence. *Biophys. J.* **2005**, *89*, 1067–1080.
19. Illya, G.; Lipowsky, R.; Shillcock, J. C. Effect of Chain Length and Asymmetry on Material Properties of Bilayer Membranes. *J. Chem. Phys.* **2005**, *122*, 244901.

20. Rawicz, W.; Olbrich, K. C.; McIntosh, T.; Needham, D.; Evans, E. Effect of Chain Length and Unsaturation on Elasticity of Lipid Bilayers. *Biophys. J.* **2000**, *79*, 328–339.
21. Szleifer, I.; Kramer, D.; Ben-Shaul, A.; Roux, D.; Gelbart, W. M. Curvature Elasticity of Pure and Mixed Surfactant Films. *Phys. Rev. Lett.* **1988**, *60*, 1966–1969.
22. Dutt, M.; Kuksenok, O.; Little, S.R.; Balazs, A.C. Designing Tunable Bio-nanostructured Materials via Self-assembly of Amphiphilic Lipids and Functionalized Nanotubes. *MRS Spring 2012 Conference Proceedings* **2012**, 1464.
23. Merkel, T. J. et al. Using Mechanobiological Mimicry of Red Blood Cells to Extend Circulation Times of Hydrogel Microparticles. *PNAS*, **2011**, *108*, 586–591.
24. Allen, T. M. Long-circulating (Sterically Stabilized) Liposomes for Targeted Drug Delivery. *Trends Pharmacol. Sci.* **1994**, *15*, 215–220.
25. Klibanov, A. L.; Maruyama, K.; Torchilin, V. P.; Huang, L. Amphipathic Polyethyleneglycols Effectively Prolong the Circulation Time of Liposomes. *FEBS Lett.* **1990**, *268*, 235–237.
26. Harris, J. M.; Chess, R. B. Effect of Pegylation on Pharmaceuticals. *Nat. Rev. Drug Discovery* **2003**, *2*, 214–221.
27. Lasic, D. D.; Woodle, M. C.; Papahadjopoulos, D. On the Molecular Mechanism of Steric Stabilization of Liposomes in Biological Systems. *J. Liposome Res.* **1992**, *2*, 335–353.
28. Blume, G.; Cevc, G. Liposomes for the Sustained Drug Release in Vivo. *Biochim. Biophys. Acta* **1990**, *1029*, 91–97.
29. Rex, S.; Zuckermann, M. J.; Lafleur, M.; Silvius, J. R. Experimental and Monte Carlo Simulation Studies of the Thermodynamics of Polyethyleneglycol Chains Grafted to Lipid Bilayers. *Biophys. J.* **1998**, *75*, 2900–2914.
30. Szleifer, I.; Gerasimov, O. V.; Thompson, D. H. Spontaneous Liposome Formation Induced by Grafted Poly (Ethylene Oxide) Layers: Theoretical Prediction and Experimental Verification. *Proc. Natl. Acad. Sci. U.S.A.* **1998**, *95*, 1032–1037.
31. Nicholas, A. R.; Scott, M. J.; Kennedy, N. I.; Jones, M. N. Effect of Grafted Polyethylene Glycol (PEG) on the Size, Encapsulation Efficiency and Permeability of Vesicles. *Biochimica Biophysica Acta* **2000**, *1463*, 167–178.
32. Garbuzenko, O.; Barenholz, Y.; Prieve, A. Effect of Grafted PEG on Liposome Size and on Compressibility and Packing of Lipid bilayer. *Chemistry and Physics of Lipids* **2005**, *135*, 117–129.
33. Lee, H.; Pastor, R. W. Coarse-grained Model for PEGylated Lipids: Effect of PEGylation on the Size and Shape of Self-assembled Structures. *J. Phys. Chem. B* **2011**, *115*, 7830–7837.
34. Sandstrom, M. C.; Johansson, E.; Edwards, K. Structure of Mixed Micelles Formed in PEG-Lipid/lipid Dispersions. *Langmuir* **2007**, *23*, 4192–4198.
35. Sandstrom, M. C.; Johansson, E.; Edwards, K. Structure of Mixed Micelles Formed in PEG-Lipid/lipid Dispersions. *Langmuir* **2007**, *23*, 4192–4198.

36. Kasbauer, M.; Lasic, D. D.; Winterhalter, M. Polymer Induced Fusion and Leakage of Small Unilamellar Phospholipid Vesicles: Effect of Surface Grafted Polyethylene-glycol in the Presence of Free PEG. *Chemistry and Physics of Lipids* **1997**, *86*, 153–159.
37. Lee, H.; Kim, H. R.; Park, J. C. Dynamics and Stability of Lipid Bilayers Modulated by Thermosensitive Polypeptides, Cholesterols, and PEGylated lipids. *Phys.Chem.Chem.Phys.* **2014**, *16*, 3763.
38. Simon, J.; Kfihner, M.; Ringsdorf, H.; Sackmann, E. Molecules *Chem. Phys. Lipids* **1995**, *76*, 241–258.
39. Nikolov, V.; Lipowsky, R.; Dimova, R. Behavior of Giant Vesicles with Anchored DNA. *Biophys J.*, **2007**, *92*, 4356–4368.
40. Seifert, U.; Lipowsky, R. Morphology of Vesicles. In: Lipowsky, R.; Sackmann, E. (eds) Structure and Dynamics of Membranes, vol 1. *Elsevier*, 1995, Amsterdam.
41. Dutt, M.; Kuksenok, O.; Nayhouse, M. J.; Little, S. R.; Balazs, A. C. Modeling the Self-Assembly of Lipids and Nanotubes in Solution: Forming Vesicles and Bicelles with Transmembrane Nanotube Channels. *ACS Nano* **2011**, *5*, 4769–4782.
42. Shi, A. C.; Li, B. Self-Assembly of Diblock Copolymers Under Confinement. *Soft Matter* **2013**, *9*, 1398–1413.
43. Stewart-Sloan, C. R.; Thomas, E. L. Interplay of Symmetries of Block Polymers and Confining Geometries. *Eur. Polym. J.* **2011**, *47*, 630–646.
44. Sushko, M. L.; Liu, J. Surfactant Two-Dimensional Self-Assembly under Confinement. *J. Phys. Chem. B.* **2011**, *115*, 4322–4328.
45. Bianchi, E.; Likos, C. N.; Kahl, G. Self-assembly of Heterogeneously Charged Particles under Confinement. *ACS Nano* **2013**, *7*, 4657–4667.
46. Yang, G.; Tang, P.; Yang, Y.; Cabral, J. T. Self-assembly of AB Diblock Copolymers under Confinement into Topographically Patterned Surfaces. *J. Phys. Chem. B.* **2009**, *113*, 14052–14061.
47. Wang, Z.; Li, B.; Jin, Q.; Ding, D.; Shi, A. -C. Self-Assembly of Cylinder-Forming ABA Triblock Copolymers under Cylindrical Confinement. *Macromol. Theor. Sim.* **2008**, *17*, 301–312.
48. Shillcock, J. C.; Lipowsky, R. Equilibrium Structure and Lateral Stress Distribution of Amphiphilic Bilayers from Dissipative Particle Dynamics Simulations. *J. Chem. Phys.* **2002**, *117*, 5048–5061.
49. West, B.; Schmid, F. Fluctuations and Elastic Properties of Lipid Membranes in the Gel L-beta State: A Coarse-grained Monte Carlo Study. *Soft Matter* **2010**, *6*, 1275.
50. Farago, O. Mode Excitation Monte Carlo Simulations of Mesoscopically Large Membranes. *J. Chem. Phys.* **2008**, *128*, 184105.
51. Farago, O. Fluctuation-induced Attraction between Adhesion Sites of Supported Membranes. *Phys. Rev. E.* **2010**, *81*, 050902.
52. Farago, O. Membrane Fluctuations near a Plane Rigid Surface. *Phys. Rev. E.* **2008**, *78*, 051919.
53. Dutt, M.; Nayhouse, M.J.; Kuksenok, O.; Little, S.R.; Balazs, A.C. Interactions of End-Functionalized Nanotubes with Lipid Vesicles: Spontaneous Insertion and Nanotube Self-organization. *Current Nanoscience* **2011**, *7*, 699-715.

54. Dutt, M.; Kuksenok, O.; Little, S.R.; Balazs, A.C. Forming Transmembrane Channels Using End-Functionalized Nanotubes. *Nanoscale* **2011**, *3*, 240-250.
55. Ludford, P.; Aydin, F.; Dutt, M. Design and Characterization of Nanostructured Biomaterials via the Self-assembly of Lipids. *MRS Fall 2013 Conference Proceedings* **2013**, 1498.
56. Koufos, E.; Dutt, M. Design of Nanostructured Hybrid Inorganic-biological Materials via Self-assembly. *MRS Spring 2013 Conference Proceedings* **2013**, 1569.
57. Smith, K. A.; Jasnow, D.; Balazs, A. C. Designing Synthetic Vesicles that Engulf Nanoscopic Particles. *J. Chem. Phys.* **2007**, *127*, 084703.
58. Goetz, R.; Lipowsky, R. Computer Simulations of Bilayer Membranes: Self-assembly and Interfacial Tension. *J. Chem. Phys.* **1998**, *108*, 7397–7409.
59. Kranenburg, M.; Venturoli, M.; Smit, B. Phase Behavior and Induced Interdigitation in Bilayers Studied with Dissipative Particle Dynamics. *J. Phys. Chem.* **2003**, *41*, 11491.
60. Kranenburg, M.; Laforge, C.; Smit, B. Mesoscopic Simulations of Phase Transitions in Lipid Bilayers. *Phys. Chem. Chem. Phys.* **2004**, *6*, 4531–4534.
61. Yamamoto, S.; Maruyama, Y.; Hyodo, S. Dissipative Particle Dynamics Study of Spontaneous Vesicle Formation of Amphiphilic Molecules. *J. Chem. Phys.* **2002**, *116*, 5842.
62. Yamamoto, S.; Hyodo, S. Budding and Fission Dynamics of Two-Component Vesicles. *J. Chem. Phys.* **2003**, *118*, 7937–7943.
63. Stevens, M. J.; Hoh, J. H.; Woolf, T. B. Insights into the Molecular Mechanism of Membrane Fusion from Simulation: Evidence for the Association of Splayed Tails. *Phys. Rev. Lett.* **2003**, *91*, 188102.
64. Stevens, M.J. Coarse-grained Simulations of Lipid Bilayers. *Chem. Phys.* **2004**, *121*, 11942–11948.
65. Arkhipov, A.; Yin, Y.; Schulten, K. Membrane-bending Mechanism of Amphiphysin N-BAR Domains. *Biophys. J.* **2009**, *97*, 2727–2735.
66. Shih, A.Y.; Arkhipov, A.; Freddolino, P. L.; Schulten, K. A Coarse-grained Protein-lipid Model with Application to Lipoprotein Particles. *J. Phys. Chem.* **2006**, *110*, 3674-3684.
67. Marrink, S. J.; Risselada, H. J.; Yefimov, S.; Tieleman, D. P.; de Vries, A. H. The MARTINI Forcefield: Coarse-grained Model for Biomolecular Simulations. *J. Phys. Chem. B.* **2007**, *111*, 7812–7824.
68. Farago, O. "Water-free" Computer Model for Fluid Bilayer Membranes. *O. J. Chem. Phys.* **2003**, *119*, 596–605.
69. Brannigan, G.; Brown, F.L.H. Solvent-free Simulations of Fluid Membrane Bilayers. *J. Chem. Phys.* **2004**, *120*, 1059.
70. Cooke, I.R.; Deserno, M. Solvent-free Model for Self-assembling Fluid Bilayer Membranes: Stabilization of the Fluid Phase based on Broad Attractive Tail Potentials. *J. Chem. Phys.* **2005**, *123*, 224710.
71. Wang, Z.; Frenkel, D. J. Modeling Flexible Amphiphilic Bilayers: A Solvent-free Off-lattice Monte Carlo Study. *Chem. Phys.* **2005**, *122*, 234711.
72. Brannigan, G.; Philips, P.F.; Brown, F.L.H. Flexible Lipid Bilayers in Implicit Solvent. *Phys. Rev. E.* **2005**, *72*, 011915.

73. Noguchi, H.; Takasu, M. Self-assembly of Amphiphiles into Vesicles: A Brownian Dynamics Simulation. *Phys. Rev. E*. **2001**, *64*, 041913.
74. Noguchi, H. Fusion and Toroidal Formation of Vesicles by Mechanical Forces: A Brownian Dynamics Simulation. *J. Chem. Phys.* **2002**, *117*, 8130-8137.
75. Katsov, K.; Mueller, M.; Schick, M. Field Theoretic Study of Bilayer Membrane Fusion I Hemifusion Mechanism. *Biophys. J.* **2004**, *87*, 3277.
76. Schick, M. *Membranes: A Field-theoretic Description*. *Encyclopedia of Biophysics*. Roberts, G.C.K., Ed., Springer-Verlag: Berlin Heidelberg, 2012.
77. May, S.; Kozlovsky, Y.; Ben-Shaul, A.; Kozlov, M.M. Tilt Modulus of a Lipid Monolayer. *Eur. Phys. J. E*. **2004**, *14*, 299–308.
78. May, S. A Molecular Model for the Line Tension of Lipid Membranes. *Eur. Phys. J. E*. **2000**, *3*, 37–44.
79. Lee, W. B.; Mezzenga, R.; Fredrickson, G. H. Self-consistent Field Theory for Lipid-based Liquid Crystals: Hydrogen Bonding Effect. *J. Chem. Phys.* **2008**, *128*, 074504–074510.
80. Ginzburg, V.V.; Balijepalli, S. Modelling the Thermodynamics of the Interaction of Nanoparticles with Cell Membranes. *Nano Lett.* **2007**, *7*, 3716–3722.
81. Ayton, G.; Voth, G. A. Bridging Microscopic and Mesoscopic Simulations of Lipid Bilayers. *Biophys. J.* **2002**, *83*, 3357-3370.
82. Wang, Z.-J.; Deserno, M. A Systematically Coarse-grained Solvent-free Model for Quantitative Phospholipid Bilayer Simulations. *J. Phys. Chem. B* **2010**, *114*, 11207.
83. Wang, Z.-J.; Deserno, M. Systematic Implicit Solvent Coarse-graining of Bilayer Membranes: Lipid and Phase Transferability of the Force Field. *New J. Phys.* **2010**, *12*, 095004.
84. Kumar, P.B.S.; Rao, M. Kinetics of Phase Ordering in a Two Component Fluid Membrane. *Mol. Cryst. Liq. Cryst.* **1996**, *288*, 105.
85. Gao, L. H.; Shillcock, J.; Lipowsky, R. Improved Dissipative Particle Dynamics Simulations of Lipid Bilayers. *J. Chem. Phys.* **2007**, *126*, 015101.
86. Laradji, M.; Kumar, P.B.S. Anomalous Slow Domain Growth in Fluid Membranes with Asymmetric Transbilayer Lipid Distribution. *Phys. Rev. E: Stat., Nonlinear, Soft Matter Phys.* **2006**, *73*, 040910.
87. Rekvig, L.; Kranenburg, M.; Vreede, J.; Hafskjold, B.; Smit, B. Investigation of Surfactant Efficiency Using Dissipative Particle Dynamics. *Langmuir*. **2003**, *19*, 8195.
88. Ilya, G.; Lipowsky, R.; Shillcock, J. C. Two-component Membrane Material Properties and Domain Formation from Dissipative Particle Dynamics. *J. Chem. Phys.* **2006**, *125*, 114710.
89. Spangler, E. J.; Laradji, M.; Kumar, P.B.S. Anomalous Freezing Behavior of Nanoscale Liposomes. *Soft Matter* **2012**, *8*, 10896-10904.
90. Revalee, J.D.; Laradji, M.; Kumar, P.B.S. Implicit-solvent Mesoscale Model based on Soft-core Potentials for Self-assembled Lipid Membranes. *J. Chem. Phys.* **2008**, *128*, 035102.
91. Groot, R. D.; Warren, P. B. Dissipative particle dynamics: bridging the gap between atomistic and mesoscopic simulation. *J. Chem. Phys.* **1997**, *107*, 4423-4435.

92. Aydin, F.; Ludford, P.; Dutt, M. Phase segregation in bio-inspired multi-component vesicles encompassing double tail phospholipid species. *2014*, *10*, 6096-6108.
93. Allen, M.P.; Tildesley, D.J. *Computer Simulations of Liquids*. Clarendon Press, Oxford, 2001.
94. Aydin, F.; Uppaladadiam, G.; Dutt, M. The design of shape-tunable hairy vesicles. *2015*, *128*, 268-275.
95. Bru, M. R.; Thompson, D. H.; Szleifer, I. Size and Structure of Spontaneously Forming Liposomes in Lipid/PEG-Lipid Mixtures. *Biophys. J.* **2002**, *83*, 2419–2439.
96. Stepniewski, M.; Gierula, M. P.; Rog, T.; Danne, R.; Orłowski, A.; Karttunen, M.; Urtti, A.; Yliperttula, M.; Vuorimaa, E.; Bunker, A. Study of PEGylated Lipid Layers as a Model for PEGylated Liposome Surfaces: Molecular Dynamics Simulation and Langmuir Monolayer Studies. *Langmuir* **2011**, *27*, 7788–7798.
97. Satulovsky, J.; Carignano, M. A.; Szleifer, I. Kinetic and Thermodynamic Control of Protein Adsorption. *Proc. Natl. Acad. Sci.* **2000**, *97*, 9037–9041.
98. Prime, K. L.; Whitesides, G. M. Self-assembled Organic Monolayers: Model Systems for Studying Adsorption of Proteins at Surfaces. *Science*. **1991**, *252*, 1164–1167.
99. Prime, K. L.; Whitesides, G. M. Adsorption of Proteins onto Surfaces Containing End-Attached Oligo (ethylene oxide): A Model System Using Self-Assembled Monolayers. *J. Am. Chem. Soc.* **1993**, *115*, 10714–10721.
100. Kim, P.; Lee, S. E.; Jung, H. S.; Lee, H. Y.; Kawai, T. Suh, K. Y. Soft Lithographic Patterning of Supported Lipid Bilayers onto a Surface and inside Microfluidic Channels. *Lab Chip*. **2006**, *6*, 54–59.
101. Duffy, D. C.; McDonald, J. C.; Schueller, O. J.; Whitesides, G. M. Rapid Prototyping of Microfluidic Systems in Poly(dimethylsiloxane). *Anal Chem.* **1998**, *70*, 4974–4984.
102. Richter, R.; Mukhopadhyay, A.; Brisson, A. Pathways of Lipid Vesicle Deposition on Solid Surfaces: A Combined QCM-D and AFM Study. *Biophys J.* **2003**, *85*, 3035–3047.
103. Li, Y.; Zhang, X.; Cao, D. The Role of Shape Complementarity in the Protein-Protein Interactions. *Sci. Rep.* **2013**, *3*, 3271.
104. Yang, K.; Vishnyakov, A.; Neimark, A. V. Polymer Translocation through a Nanopore: DPD Study. *J. Phys. Chem. B* **2013**, *117*, 3648–3658.
105. Somani, S.; Shaqfeh, E. S. G.; Prakash, J. R. The Effect of Solvent Quality on the Coil-stretch Transition. *Macromolecules* **2010**, *43*, 10679–10691.
106. Kučerka, N.; Nieh, M.P.; Katsaras, J. Fluid Phase Lipid Areas and Bilayer Thicknesses of Commonly Used Phosphatidylcholines as a Function of Temperature. *J. Biochim. Biophys. Acta.* **2011**, *1808*, 2761–2771.
107. Seifert, U.; Berndl, K.; Lipowsky, R. Shape Transformations of Vesicles: Phase Diagram for Spontaneous-curvature and Bilayer-coupling Models. *Phys. Rev. A.* **1991**, *44*, 1182.
108. Lipowsky, R.; Dimova, R. Domains in Membranes and Vesicles. *J. Phys.: Condens. Matter*, **2003**, *15*, 31–45.

109. Shinoda, W.; Discher, D. E.; Klein, M. L.; Loverde, S. M. Probing the Structure of PEGylated-lipid Assemblies by Coarse-grained Molecular Dynamics. *Soft Matter* **2013**, *9*, 11549.
110. Lifshitz, I. M.; Slyozov, V. V. The Kinetics of Precipitation from Supersaturated Solid Solutions. *J. Phys. Chem. Solids* **1961**, *19*, 35-50.
111. Helal, K.; Biben, T.; Hansen, J. -P. Influence of Capillary Confinement on the Equilibrium Shape of Vesicles. *J. Phys.: Condens. Matter*. **1999**, *11*, 51–58.
112. Lipowsky, R.; Sackmann, E. Structure and Dynamics of Membranes, Handbook of Biological Physics. *Elsevier*, Amsterdam, 1995.
113. Dobereiner, H.-G.; Evans, E.; Kraus, M.; Seifert, U.; Wortis, M. Mapping Vesicle Shapes into the Phase Diagram: A Comparison of Experiment and Theory. *Phys. Rev. E*. **1997**, *55*, 4458.
114. Nieh, M.P.; Pencer, J.; Katsaras, J.; Qi, X. Spontaneously Forming Ellipsoidal Phospholipid Unilamellar Vesicles and Their Interactions with Helical Domains of Saposin C. *Langmuir* **2006**, *22*, 11028-11033.
115. Du, H.; Chandaroy, P.; Hui, S.W. Grafted poly-(ethylene glycol) on lipid surfaces inhibits protein and cell adhesion. *Biochim. Biophys. Acta (BBA)—Biomembranes*, **1997**, *1326*, 236-248.
116. Patel, H.M. Serum opsonins and liposomes: their interaction and opsonophagocytosis. *Crit. Rev. Ther. Drug Carr. Syst.*, **1992**, *9*, 39-90
117. Bonte, F.; Juliano, R.L. Interactions of liposomes with serum proteins. *Chem. Phys. Lipids*, **1986**, *40*, 359-372.
118. Knight, C.G. Liposomes from Physical Structure to Therapeutic Applications, *Elsevier/North-Holland*, Amsterdam, 1981.
119. Oja, C.D.; Semple, S.C.; Chonn, A.; Cullis, P.R. Influence of dose on liposome clearance: critical role of blood proteins. *Biochim. Biophys. Acta*, **1996**, *1281*, 31-37.
120. Semple, S.C.; Chonn, A.; Cullis, P.R. Influence of cholesterol on the association of plasma proteins with liposomes. *Biochemistry*, **1996**, *35*, 2521-2525.
121. Pozzi, D.; Colapicchioni, V.; Caracciolo, G.; Piovesana, S.; Capriotti, A. L.; Palchetti, S.; de Grossi, S.; Riccioli, A.; Amenitsch, H.; Lagana, A. Effect of polyethyleneglycol (PEG) Chain Length on the Bio-nano-interactions between PEGylated Lipid Nanoparticles and Biological Fluids: from Nanostructure to Uptake in Cancer Cells. *Nanoscale* **2014**, *6*, 2782-2792.
122. Price, M. E.; Cornelius, R. M.; Brash, J. L. Protein Adsorption to Polyethylene Glycol Modified Liposomes from Fibrinogen Solution and from Plasma. *Biochim. Biophys. Acta* **2001**, *1512*, 191-205.
123. Nuytten, N.; Hakimhashemi, M.; Ysenbaert, T.; Defour, L.; Trekker, J.; Soenen, S. J.; van der Meeren, P.; De Cuyper, M. PEGylated Lipids Impede the Lateral Diffusion of Adsorbed Proteins at the Surface of (Magneto) Liposomes. *Colloids Surf. B Biointerfaces* **2010**, *80*, 227-231.
124. Wang, B.; Zhang, L.; Bae, S.C.; Granick, S. Nanoparticle-induced Surface Reconstruction of Phospholipid Membranes. *PNAS* **2008**, *105*, 18171-18175.
125. Santos, N.D.; Allen, C.; Doppen, A.M.; Anantha, M.; Cox, K.A.K.; Gallagher, R.C.; Karlsson, G.; Edwards, K.; Kenner, G.; Samuels, L.; Webb, M.S.; Bally, M.B. Influence of poly(ethylene glycol) grafting density and polymer length on

- liposomes: relating plasma circulation lifetimes to protein binding. *Biochim. Biophys. Acta*, **2007**, *1768*, 1367–1377
126. Song, Y.; Chen, S. Janus Nanoparticles: Preparation, Characterization, and Applications. *Chem. Asian J.* **2014**, *9*, 418-430.
127. Szleifer, I. Protein Adsorption on Surfaces with Grafted Polymers: A Theoretical Approach. *Biophys. J.* **1997**, *72*, 595-612.